TABLE OF CONTENTS

LIST OF FIGURES

LIST OF TABLES

1 DEFINITION OF THE PROBLEM

1.1 Introduction

Pure aluminum obtained from the electronic reduction of Alumina (Al_2O_3) is a relatively weak material. Therefore, for applications requiring greater mechanical properties, aluminum is alloyed with other alloying elements such as copper, zinc, magnesium and manganese, usually in combinations of two or more of these elements together with iron and silicon. Aluminum alloys have traditionally been associated with applications in the automobile and aerospace industries, because their specific strengths (strength-to-weight ratios) are outstanding compared to both engineering alloys of other metals, and other engineering materials in general. The advantages of decreased density become even more important in engineering design for parameters such as stiffness and resistance to buckling. Concern with aspects of weight saving should not obscure the fact that the aluminum alloys possess other properties of considerable technological importance, e.g. the high corrosion resistance and good electrical and thermal conductivities.

2xxx series heat-treatable aluminum alloys, based upon the Al-Cu-Mg alloy system, are widely employed in aerospace and automobile applications requiring a combination of high strength and ductility [1]. However, the mechanical properties of these alloys decrease significantly when they are exposed at temperature more than 100 °C [2]. Aluminum alloy 2618 is an Al-Cu-Mg alloy containing certain amount of Fe and Ni. The addition of Fe and Ni to this alloy was found to improve its performance in applications involving high temperature exposures up to 300 °C, such as engines for both automotive and aircraft applications [3].

Recently, DC cast aluminum ingot plates have been increasingly used for large mold manufacturing to take the advantage of the available larger material dimensions combined with superior mechanical properties and excellent dimensional stability. Moreover, these plates are cut directly from the ingots and used in the non-deformed condition, *i.e.* without hot and/or cold rolling usually applied to wrought alloys, which reduces production costs and processing time. AA2618 DC cast alloy has received particular attention from large mold manufacturers owing to its excellent machinability, good weldability, and high stability of mechanical properties at elevated temperatures. This alloy was originally employed as a wrought alloy, so most of the existing research works have focused on the alloy microstructure and mechanical properties after

deformation processes such as forging, rolling and extruding. On the other hand, little research work has been done on the application of the AA2618 alloy in the non-deformed condition. The influence of heat treatment procedures on the microstructures and mechanical properties of the non-deformed AA2618 cast alloy, which represents important factors for the industry of molding plates, is still unknown and therefore needs intensive research work.

1.2 Objectives

The present work is undertaken to study the effects of heat treatment on the microstructure and mechanical properties of non-deformed AA2618 DC cast alloy, proposed for the manufacturing of molding plates, in order to find the optimum heat-treatment procedures that can be applied to this alloy. In keeping with this aim, the objectives of the intended study will include the following points:

1. Identifying the intermetallic phases contained in the as-cast alloy microstructure;

2. Studying the effects of various heat treatment procedures, namely solution treatment, quenching and aging, on the microstructure and mechanical properties of the alloy;

3. Investigating the precipitation characteristics of the AA2618 alloy under different aging conditions.

2 LITERATURE REVIEW

2.1 Al-Cu-Mg alloys

2xxx series aluminum alloys, whose principal alloying element is copper (Cu), are used in many applications for their particular combinations of strength and corrosion resistance. In aerospace and automobile industries, the high strength-to-weight ratio, which is particularly important in the design of structural components, makes these alloys a very attractive class of materials. Among the present 2xxx series aluminum alloys, alloy 2014 and 2024 are widely used in aircraft structures, rivet hardware, truck wheels, screw machine products, and other miscellaneous structural applications because of their good performance below 100 °C [4].

2xxx series Al-Cu-Mg alloys date from the accidental discovery of the age hardening phenomenon by Alfred Wilm in 1906, who was seeking to develop a stronger aluminum alloy to replace brass for the manufacture of cartridge cases. His work led to the production of an alloy known as Duralumin (Al-3.5Cu-0.5Mg-0.5Mn) which has

better properties and was quickly used in aircraft construction. Later, several other important alloys were developed and widely used in aircraft industry. One example is 2014 alloy (Al-4.4Cu-0.8Si-0.8Mn-0.5Mg) which achieved higher strength because the relatively high silicon content increases the response to hardening during artificial aging process. The typical tensile properties of this alloy are: 0.2% yield strength of 414 MPa and tensile strength of 483 MPa [4]. Another alloy 2024, in which the Mg content is raised to 1.5% and the Si content is reduced to impurity levels, exhibits significant hardening by natural aging at room temperature and is frequently used in T3 or T4 tempers.

2.2 AA2618 alloy

Aluminum alloy 2618 (also known as RR58) is an Al-Cu-Mg alloy having chemical composition listed in Table 2.1. Addition of Fe and Ni to this alloy was found to improve its elevated temperature performance up to 300 °C as shown in Figure 2.1 [5]. AA2618 is frequently used for high temperature applications in automotive and aerospace industries and has been successfully used as the primary structure of the supersonic Concorde airplane [3].

Table 2.1 Typical chemical composition of 2618 alloy [4].

Alloy	Cu	Mg	Fe	Ni	Si	Zn	Ti	others	Al
2618	1.9-2.7	1.3-1.8	0.9-1.3	0.9-1.2	0.1-0.25	<0.10	0.04-0.1	<0.15	Bal.

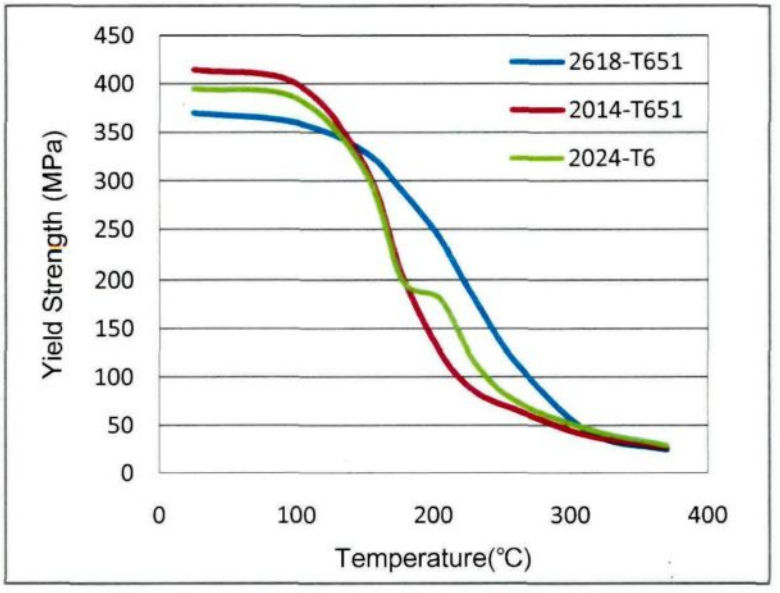

Figure 2.1 Values of 0.2% yield strength of 2xxx aluminum alloys after exposure for 1000 h (data from Ref [5]).

2.2.1 Effects of nickel and iron in 2618 alloy

The addition of certain amounts of Fe and Ni in 2618 alloys could produce microstructural stability under thermal exposure [6], and thus retain the high strength

property even applied at elevated temperatures.

2.2.1.1. Effect of nickel

Nickel is a corrosion-resistant metal with a high melting temperature (1453°C). It exhibits good ductility due to its face-centered cubic (f.c.c.) crystal structure. Nickel can be readily alloyed with other metallic elements to form a wide range of commercial alloys which are used in a multiplicity of consumer applications, including household appliances, electronics, and automotive components. They are also used in critical industrial technologies such as chemical processing, pollution control, aircraft and missile propulsion, and electric power generation.

The solid solubility of nickel in aluminum does not exceed 0.04%. Over this amount, it is present as an insoluble intermetallic, usually in combination with iron. Nickel amount up to 2% increases the strength of high-purity aluminum but reduces ductility. Binary Al-Ni alloys are no longer in use but Ni is added to Al-Cu and Al-Si alloys to improve hardness and strength at elevated temperatures and to reduce the coefficient of expansion [6].

Alloy Y, the first of the Ni-containing light aluminum alloys, was developed by the

National Physical Laboratory during World War I, in attempt to find an aluminum alloy that would retain its strength at high temperatures. Like duralumin, this was a 4% copper alloy, but with the addition of 2% nickel and 1.5% magnesium [7]. As for many of the aluminum alloys, Y alloy can be age hardened spontaneously at normal temperatures after solution heat treatment. The heat treatment consists of solution treatment at 500-520 °C for 6 h, then natural aging for 7–10 days [8]. The precipitation hardening that takes place during this aging forms precipitates of both $CuAl_2$ and $NiAl_3$ [7].

Wilson and Forsyth [9] investigated the effects of adding 1 wt.% nickel to an age-hardening Al-2.5%Cu-1.2%Mg alloy and found that the nickel formed an intermetallic phase which was present from the casting stage and was insoluble at the solution-treatment temperature. After forging and rolling, the as-cast structure was broken down and the insoluble phase dispersed in the form of small spherical particles (0.5-1 μm dia.) throughout the matrix. A comparison of the final grain size achieved in the alloys after solution-treatment showed that the nickel-bearing alloys had resisted grain growth, and thin-foil transmission electron microscopy revealed that many grain boundaries were pinned by the nickel-rich particles.

According to the mechanical testing results shown in Figure 2.2, nickel, however,

lowers the hardness values of the alloy, since the addition of nickel has decreases the age-hardening ability of the alloy by forming an insoluble Ni-Cu phase, thereby preventing copper from entering into solid solution. Underhill *et al.* [10] reported the existence of Al_7Cu_4Ni phase particles in spray-formed AA2618 alloy.

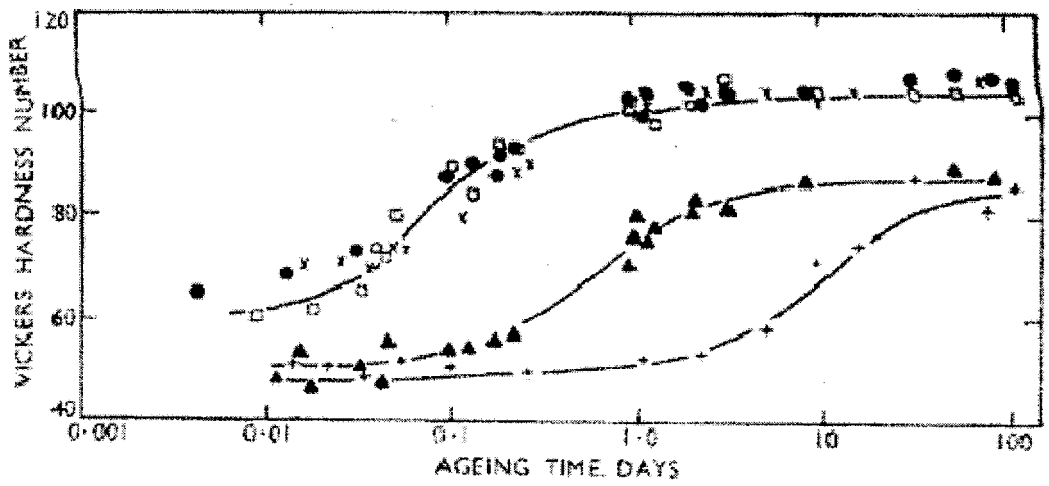

(a)

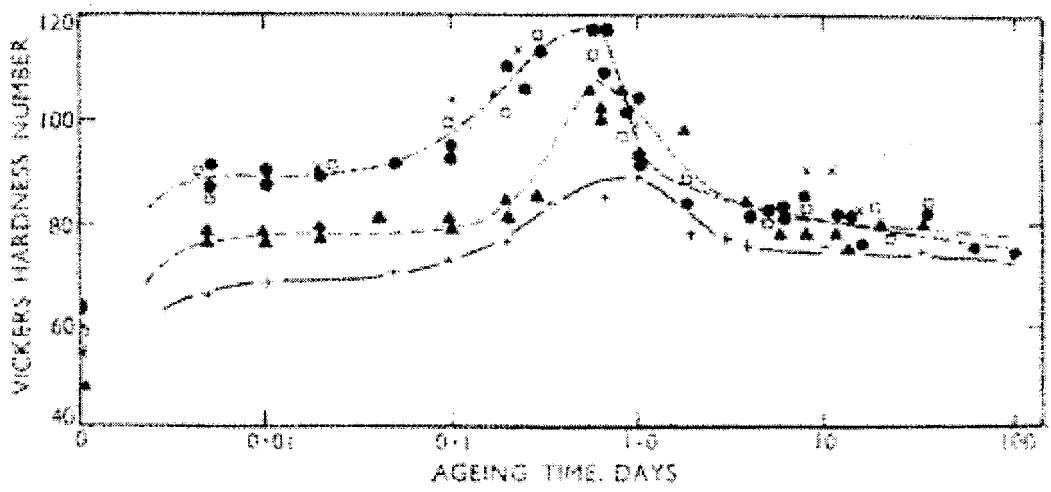

(b)

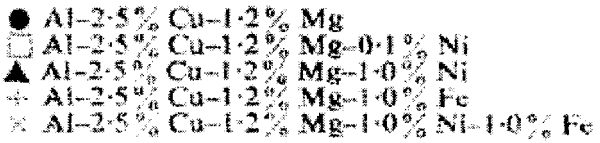

Figure 2.2 The effects of Fe and Ni on the hardness values of an Al-2.5Cu-1.2Mg alloy for different aging times at: (a) room-temperature and (b) 190 °C [9].

2.2.1.2. Effect of iron

Iron is usually an impurity in aluminum alloys and forms a constitute, $FeAl_3$, that is essentially insoluble in solid aluminum and frequently appears as a coarse, insoluble constituents with many other alloying elements that may be present, including Cu, Ni, Mn and Si. These coarse phases reduce ductility and induce cracking of wrought alloys during fabrication.

The cast Al-Cu-Mg alloys containing iron are characterized by dimensional stability and improved bearing characteristics, as well as by high strength and hardness at elevated temperatures. However, in a wrought Al-4Cu-0.5Mg alloy, iron in concentrations as low as 0.5% distinctly lowers the tensile properties in the heat treated condition, if the silicon content is less than that required to tie up the iron as the α-FeSi constitute [6]. In this case, the excess iron combines with copper to form the Al_7Cu_2Fe phase, thereby reducing the

amount of copper available for age hardening effects. When sufficient silicon is present to combine with the iron, the properties are unaffected [6].

Wilson and Forsyth [9] also found that the effect of the addition of 1% iron upon the age hardening of the Al-2.5%Cu-1.2%Mg alloy was similar to that of 1% nickel, as shown in Figure 2.2.

2.2.2 Effects of combined additions of Ni and Fe

When 1% Ni and 1% Fe were added together into the Al-Cu-Mg alloy, the age-hardening behaviour at both room and elevated temperature restored to that of the ternary alloy, as shown in Figure 2.2. This observation can be explained in terms of the fact that the combined addition of Ni and Fe forms the low Cu content Al_9FeNi intermetallic phase and therefore allows the full Cu content of the alloy to enter into solid solution, which in turn improve the age-hardening process. This phase also provides insoluble particles which stabilize the grain size by pinning the grain boundaries, and as a result the grain growth is restricted in high temperature applications.

Feng *et al.* [11] and Wang *et al.* [12] investigated the microstructure of the as-cast Al-2.24Cu-1.42Mg-0.9Fe-0.9Ni alloy and found that the microstructures of the as-cast

alloy consist of α-Al matrix as well as Al_2CuMg, Al_2Cu, Al_9FeNi, Al_7Cu_2Fe and Al_7Cu_4Ni intermetallic phases

Oguocha *et al.* [13] reported the Al_xFeNi phase in cast AA2618alloy has a C-centered monoclinic structure and the structural formula of this phase varies from particle to particle according to the aluminum content.

2.2.3 Effects of other additives on 2618 alloy

The mechanical properties of age-hardening aluminum alloys could be greatly affected by slight variations in chemical composition. Other alloying elements were added to 2618 alloy by other researchers to promote the comprehensive properties.

Bergsma *et al.* [14] compared the ambient and elevated-temperature T6 tensile properties of "air slip" cast aluminum alloy ingot 2618 and 2618 alloyed with additional Cu as well as some additional Mn, Fe and Ni. They found that the addition of alloying elements appears to increase strength slightly, but to decrease ductility at ambient temperature.

Trace additions of Si modify the aging process and sequence in Al-Cu-Mg alloys. Addition of 0.25 wt% Si enhances the artificial age hardening of Al-2.5wt%Cu

-1.5wt%Mg and Al-2.5wt%Cu-1.2wt%Mg alloys, but does not affect the time to peak hardness. However, Si additions retard the age hardening at room temperature due to preferential interaction of vacancies with Si atoms [15]. Precipitation of other phases, such as θ-Al_2Cu, is also possible in alloys with higher Si contents in which Mg_2Si forms in greater amounts, thereby consuming more Mg from the matrix [16].

The microstructure and mechanical properties of 2618 alloy with 0.5wt% of Ti were investigated by Wang *et al.* [17]. When Ti is used as an alloying element, it does not affect the morphology of Al_9FeNi phase in cast alloy, but decreases the grain size of as-cast alloy remarkably. The grain size of quenched-aged 2618 alloy decreases apparently due to the existence of a great deal of dispersive Al_3Ti particles. The addition of 0.5%Ti has no effect on the tensile properties of 2618 alloy at room temperature, but apparently increases its elevated temperature instantaneous tensile properties at 250 °C, as well as those when the alloy is exposed to 250 °C for long time up to 100 h. This is attributed to the formation of the dispersive Al_3Ti particles which are stable at high temperatures.

Effects of combined additions of Sc and Zr on microstructure and mechanical properties of 2618 alloy were studied by Yu *et al.* [18]. It was found that the addition of

Sc and Zr to 2618 alloy results in the formation of the primary $Al_3(Sc, Zr)$ phase. Such phase could refine the grain structure of the alloy because it acts as a heterogeneous nucleation sites during solidification. The secondary $Al_3(Sc, Zr)$ phase particles, that precipitate from the α(Al) solid solution, are fully coherent with the matrix and have an obvious precipitation hardening effect. These particles also made the distribution of *S'* phase precipitates more homogeneous. The strength of the 2618 alloy containing $Al_3(Sc, Zr)$ phase increases at both ambient and elevated temperatures, without a decrease in ductility.

2.3 Solution heat treatment

Heat treatment is a traditional and essential metallurgical technique widely used to improve the mechanical properties of heat-treatable aluminum alloys. The heat treatment procedures of AA2618 alloy are similar with other 2xxx series alloys and will be discussed below.

The purpose of the solution heat treatment is to obtain a solid solution containing the maximum possible concentration of the hardening solutes such as Cu, Mg, Si, or Zn. The Al-rich portion of Al-Cu binary phase diagram shown in Figure 2.3 reveals that the solubility of Cu in α-Al increases obviously with temperature and reaches to maximum

(5.65 wt. %) at the eutectic melting temperature (548 °C). The rate of solution increases with temperature, because of increased diffusion rate. According to the Al-Cu binary phase diagram, it could be found that the theoretical solution temperature for AA2618 alloy containing 2.4 wt. % copper ranges from 440 °C to 548 °C.

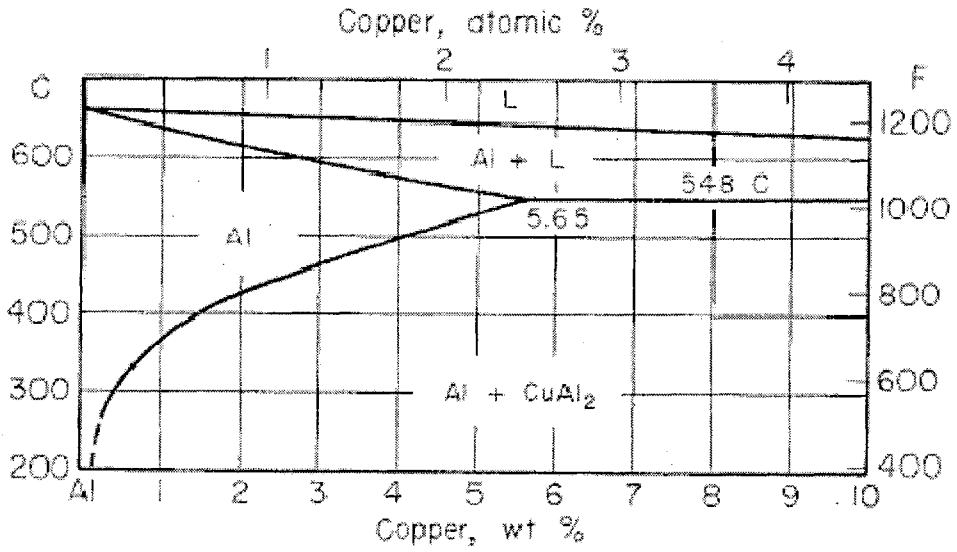

Figure 2.3 Al-rich portion of Al-Cu binary phase diagram [19].

The influence of solution heat treatment temperature on the tensile properties of 2014 alloy for both T4 and T6 aging treatments are shown in Figure 2.4. At low temperatures, alloying elements are not dissolved completely into the matrix which may reduce the effect of precipitation hardening. On the other hand, the high solution

treatment temperature causes incipient melting of second phases leading to intergranular networks of nonductile eutectic which in turn decreases both strength and ductility. Liu *et al.* [20] observed that the mechanical properties of Al-Cu-Mg-Ag alloy increase first and then decrease with increasing the solution temperature.

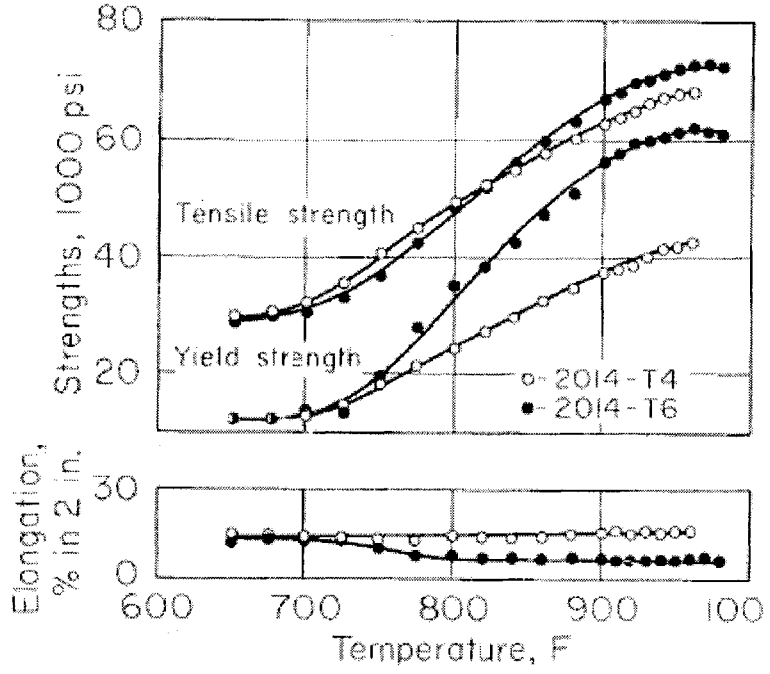

Figure 2.4 Effects of solution temperature on the tensile properties of 2014-T4 and 2014-T6 sheet [21].

Given that the nominal temperatures specified for commercial solution heat treatments of many alloys are only 10 to 15 °C below the eutectic temperature, good control and uniformity of temperature within furnaces are essential. However, compared

to the solution temperature, the solution holding time has less effect on the microstructure and the mechanical properties.

2.4 Quenching

Quenching after solution treatment is a very critical step in the sequence of heat treatment practice. The objective of quenching is to preserve as nearly intact as possible the solid solution formed at the solution heat treating temperature, by rapid cooling to lower temperature, usually near to room temperature.

The cooling rate has a significant impact on the precipitation strengthening of alloys. Figure 2.5 illustrates the tensile strength variation tendency of different alloys as a function of cooling rate during quenching. When the cooling rate is lower than 100 °F per sec, the tensile strength decreases obviously and the reduction in strength for a specific decrease in cooling rate differs from one alloy composition to another [19]. This sensitivity to the quench path is attributed primarily to loss of solute by heterogeneous nucleation and growth of quench precipitates which do not provide strengthening during subsequent aging [22].

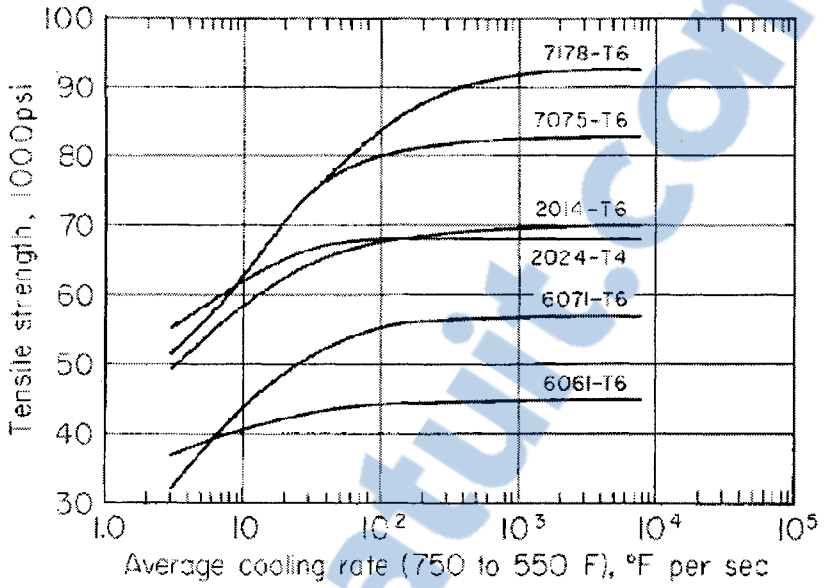

Figure 2.5 Tensile strengths of six alloys as a function of average cooling rate during quenching [19].

There are two main factors that determine the cooling rate of alloys: product size and shape, and quenching medium.

The rate of cooling is a function of the ratio of surface area to volume, since heat transfer during quenching basically is limited by the resistance at the surface in contact with the quenching medium. In the case of sheets and plates, as well as other products of similar shape, average cooling rates vary with product thickness in a relatively simple manner and the relation can be approximated by the following equation [19]:

$$\text{Log } r_t = \log r_1 - k \log t \quad (1)$$

where r_t= average cooling rate at thickness t in °F per sec; r_1= average cooling rate at 1 in. thickness in °F per sec; and k = constant.

As quenching medium concerned, water is not only the most widely used medium but also the most effective. Figure 2.6 shows cooling rates determined experimentally for different thick sections that were quenched by immersing in water at five different temperatures and by cooling in still air. It could be observed that the cooling rate decreases with increasing section thickness of products [19]. Moreover, in water quenching, cooling rates can be reduced by increasing water temperature. Figure 2.7 shows the average tensile properties of 7075 plate as a function of plate thickness [19].

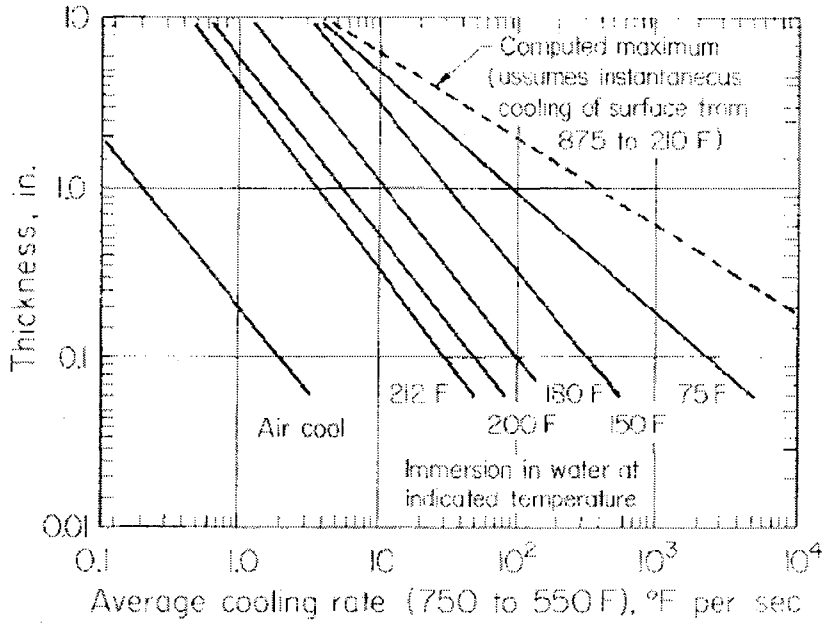

Figure 2.6 Effects of thickness and quenching medium on average cooling rates [19].

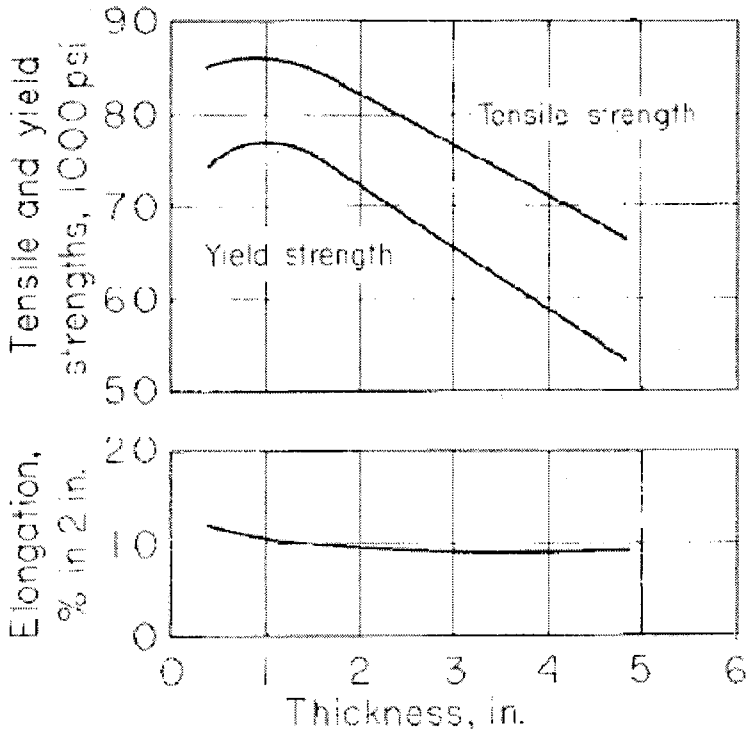

Figure 2.7 Average tensile properties of 7075-T651 plate as a function of thickness [19].

AA2618 aluminum alloy is a quench sensitive alloy [23]. Cooling rate is a very important factor in the manufacturing and post-fabrication processes of AA2618 aluminum alloy. In particular, it equally affects the as-quenched and aged properties of this alloy. However, it does not alter the precipitation sequence of AA2618 aluminum, i.e., the precipitation sequence is independent of the quenchant used [23].

The effect of quenching conditions on final properties, which is known as quenching sensitivity, could be determined using the Jominy end quench test [24-26]. The Jominy end quench test, which is well known as a method of measuring hardenability in steels, offers a method for studying many quenching conditions with a minimum of samples. In the original classic work by Jominy and Boegehold [27], a cylindrical specimen, 100 mm long by 25 mm in diameter, as shown in Figure 2.8, was austenitized and then removed from the furnace and placed in a fixture, where the specimen was exposed at one end to a specified vertical stream of water. The resulting cooling is one dimensional and the cooling rate decreases with increasing distance to the quench end.

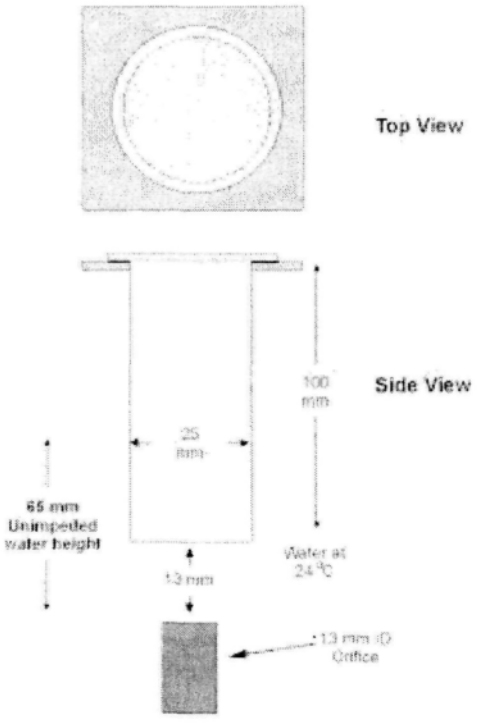

Figure 2.8 Schematic of the Jominy end quench.

Loring *et al.* [28] authored the first published paper on the use of the Jominy end quench test for studying aluminum alloys using a modified L-type Jominy specimen. The cooling curves at various distances up to 25 mm were measured. Different types of aluminum (14S, 24S, 61S, R-301, and 75S) were tested. Hardnesses were measured at 3 mm intervals using the Rockwell B, F, and Vickers (5 kg) scales. Further, it was seen that higher quench rates yielded decreasing hardness in the as-quenched condition. Low cooling rates produced relatively small changes in the hardness. Only 75ST exhibited a sensitivity to quench rate after aging. Newkirk *et al.* [24] found that AA7075 aluminum

alloy is very quench sensitive, of whom the Vickers hardness of the cross-section area decreases significantly with increasing distance from the quenched end of the quench bar.

2.5 Precipitation hardening

After solution treatment, a supersaturated solid solution is obtained. At room temperature or higher temperature, some of the solute atoms will react with some of the solvent atoms to form precipitate particles, since the practical content is higher than the solubility limit at this temperature. These fine precipitates will obstruct the movement of dislocations and therefore improve the mechanical properties of materials.

Hardy [29] examined the aging behavior of an Al-4Cu alloy. The alloy was solution heat treated for at least 48 h at 520 °C, then water quenched to 20 °C. The hardness is measured as a function of aging time as shown in Figure 2.9.

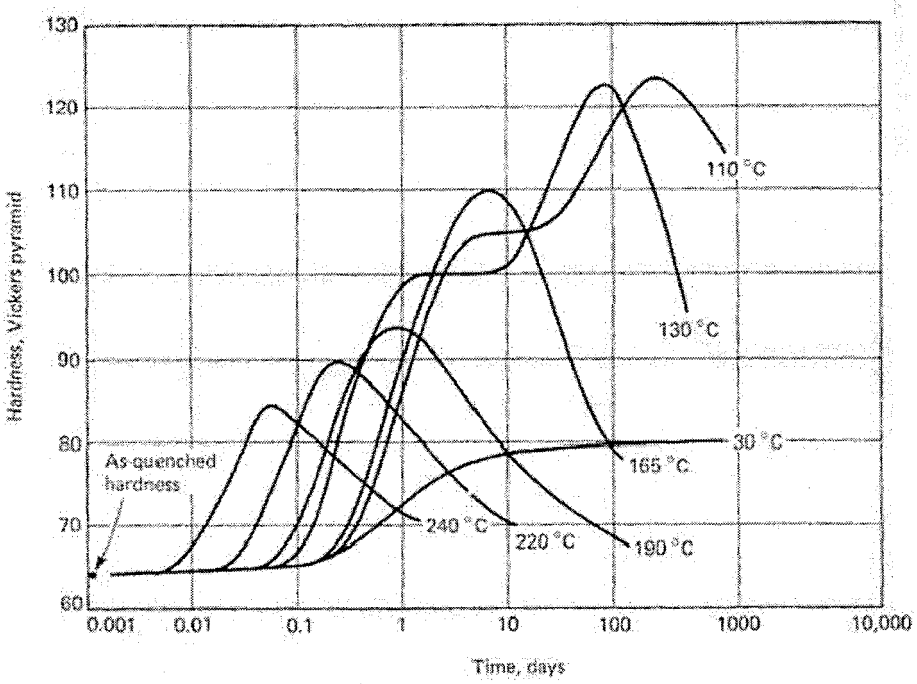

Figure 2.9 Hardness as a function of aging time for an Al-4Cu alloy [29].

Note that the hardness curves pass through a maximum value, and are quite temperature dependent. The maximum hardness, which is known as the peak aging point or T6 temper, is associated with precipitates attaining a critical size and distribution. When the precipitates become too coarsened, they are too dispersed to be as effective in retarding dislocation motion, and hardness decreases. The formation of the precipitates to an optimum size and distribution will be more rapid at higher temperature, so that the peak hardness occurs at shorter time as the aging temperature increases. However, the amount of the precipitate formed decreases with increasing temperature (the degree of

supersaturation decreases), and the magnitude of the peak hardness decreases. Also, it is expected that at a given aging temperature, the higher the solute content, the faster the peak hardness will be attained, because the supersaturation will be greater, and therefore diffusion will be faster.

2.5.1 Precipitation sequence

In Al-Cu binary alloys, the precipitation sequence can be represented as: supersaturated solid solution ⟶ GP zones ⟶θ'' ⟶θ' ⟶θ (Al_2Cu), while in Al-Cu-Mg alloys, the precipitation sequence is still in dispute.

Bagaryatsky [30] first proposed the precipitation sequence during the artificial aging of Al-Cu-Mg alloys as supersaturated solid solution (SSSS) ⟶ zones ⟶S" ⟶ S' ⟶ S. The zones, which are coherent with the matrix and enriched with Cu and Mg, were named as the Guinier-Preston-Bagaryatsky (GPB) zones by Silcock [31]. Bagaryatsky [30] considered the GPB zone as a short-range ordering of Cu and Mg solute atoms. The structure of S" has not been clearly confirmed. The ternary S phase with a composition of Al_2CuMg has been determined as an orthorhombic structure with lattice parameters a = 0.400 nm, b = 0.923 nm, c = 0.714 nm by Perlitz and Westgren [32] (P-W) on the basis of X-ray diffraction (XRD) work. The S' phase has generally been

considered as semi-coherent with the matrix. As the S' phase possesses the same structure as the S phase with slightly difference in lattice parameters, it is now regarded that there is no distinction between the S' and S phases [33, 34].

Since the mid-1990s, atom probe field ion microscopy (APFIM) and three-dimensional atom-probe (3DAP) have evidenced that the first stage of age hardening is due to the formation of co-clusters [35, 36]. Ringer *et al.* [37] proposed the following 3-stage precipitation sequences for the ageing of Al–Cu–Mg alloys:

SSSS ⟶ Cu-Mg co-clusters ⟶ GPB zone ⟶ S

where the Cu–Mg co-clusters are responsible for the initial hardening, GPB zone is the dominant precipitate at peak strengthening and the S phase appears in the softening stage. However, Gao *et al.* [38] and Wang *et al.* [33] found that the peak aging is dominated by the formation of S precipitates and no significant amounts of other phases or zones are detected.

The structural changes occurring at room temperature differ in fundamental ways from those occurring at elevated temperatures [6]. However, information about the microstructure evolution during natural aging is scarce. Starink [36] found that

strengthening due to modulus hardening generated by the difference in shear modulus of Cu–Mg co-clusters and matrix is the main strengthening mechanism for room temperature hardening of Al-Cu-Mg alloys. The early stages of natural ageing in laboratory Al–Cu–(Mg) alloys and in AA2024 were investigated using positron annihilation and X-ray absorption spectroscopy by Klobes *et al.* [39] who also concluded that the natural aging hardening process was associated with the growth of co-clusters and no S″ phase formed during natural aging in the investigated Al-Cu and Al-Cu-Mg alloys.

2.5.2 Precipitation hardening of AA2618

Figure 2.10 shows AA2618 alloy situated in the $\alpha + \theta +$ S phase field of the Al-Cu-Mg phase diagram. During the aging process, both θ and S phases precipitate out of the solid solution and strengthen the alloy. The fractions of these two phases depend on the concentration ratio of Cu to Mg, as well as their total content. However, according to other research works [40, 41], the main strengthening phase in AA2618 alloy is S phase.

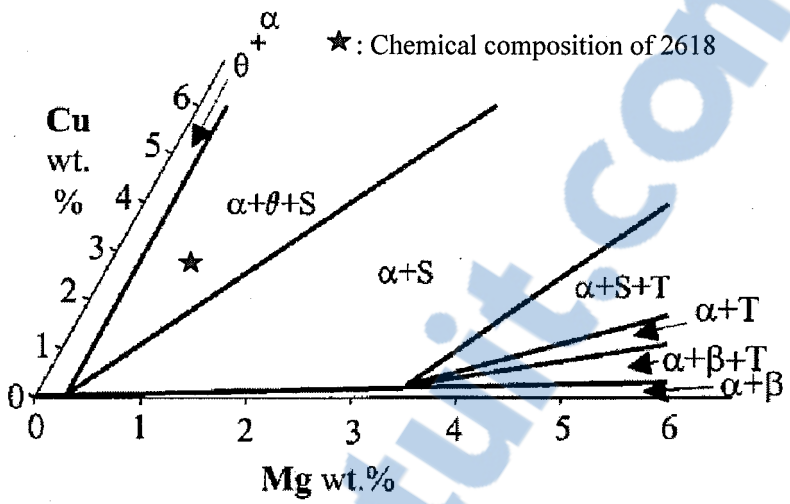

Figure 2.10 Isothermal section of ternary Al-Cu-Mg phase diagram at 200 °C [42];

($\alpha = Al$, $\theta = CuAl_2$, $S = Al_2CuMg$, $T = Al_6CuMg_4$ and $\beta = Al_{12}Mg_{17}$).

Novy *et al.* [41] examined the microstructure of T6-AA2618 alloys and found that the microstructure of the alloy in the peak aging condition consists of polyhedric grains of the solid solution of α-Al containing Cu and Mg. The Al_9FeNi, Al_2CuMg, Mg_2Si, AlCuNi and Al_7Cu_2Fe intermetallic phases were identified in the microstructure. The majority of the intermetallic phases found, however, belong to the phase Al_9FeNi. This phase significantly improves mechanical properties and reduces the undesirable grain growth at high temperatures. The main strengthening *S*-Al_2CuMg phase was distributed uniformly in the form of tiny plate-like precipitates (GPBII zones) of the approximate

size of 50 nm in grain interior.

Lu *et al.* [16] found that prior natural aging of 2618 alloy weakened the hardening in the subsequent artificial aging at 180, 200, and 230 °C, but had no such effect at 150 °C. The decrease in hardness at 180, 200, and 230 °C is due to the cluster reversion that delays the precipitation of strengthening phases. On the contrary, at 150 °C, the clusters survive and age hardening proceeds with no delay.

2.5.3 Effects of precipitates on the electrical conductivity

Electrical conductivity measurements, employing eddy current techniques, are often utilized in order to determine the kinetic behaviour of the precipitation process or to evaluate the progress of the age hardening sequence non-destructively [43-45]. The variation in the electrical conductivity with aging is complex and results from a number of contributions [46] including changes in the scattering of conduction electrons from (1) the vacancies quenched in during the rapid cooling after solution heat treatment, (2) the alloying atoms present in the matrix, (3) the Guinier-Preston (GP) zones with dimensions comparable with the electron wavelength and (4) the boundaries of the zones or clusters [47].

Many aluminum alloys are unstable for a considerable period of time after solution heat treatment even if held at room temperature. During this time, a certain amount of atom migration takes place to initiate the formation of sub-microscopic particles. During this process, sometimes called natural aging, two competing processes occur. There is a decrease in the number of quenched-in vacancies and a clustering of copper and magnesium atoms which tend to increase the conductivity. Simultaneously, there is a more significant decrease in the electrical conductivity due to the appearance of newly formed clusters, or precipitates, small enough to be effective as scatterers of electrons. Under the combination effect of these two competing processes, the electrical conductivities of natural aged samples yield a decreasing tendency with increasing aging time [47].

If a solution heat treated alloy is precipitation hardened by heating at relatively higher temperature, that is, artificially aging hardened, alloying atoms form small particles. At a critical size and distribution of particles, the strength of the aluminum alloy reaches a maximum. Electrical conductivity also increases during the precipitation hardening or artificial aging process [48, 49]. If aging is carried on beyond the point where optimum strength is obtained, strength will decrease, while conductivity will continue to increase to an ultimate value determined by the solubility of impurity atoms

at the specific aging temperature. The absolute value of electrical conductivity achieved after any given aging time is dependent on aging temperature owing to the fact that the geometry and size distribution of the precipitates are governed by a thermally activated process [50].

Rosen and Horowitz [47] found that there is an initial decrease in conductivity at each of the isothermal aging temperatures in the range between 21 and 190 °C, as shown in Figure 2.11. For specimens aged in the temperature range between 150 and 190 °C, the rate of initial decrease in conductivity is virtually identical. They also observed that in contrast with the decreasing tendency in the electrical conductivity as a function of aging time at low temperature (below 50 °C), the conductivity above 150 °C increases with increasing isothermal aging temperature after the initial decrease during the first 5 min of the aging process.

Tariq *et al.* [51] observed that electrical conductivity measurement results of AA2014, AA2024 and AA2219 aluminum alloys exhibited a linear trend, that is, conductivity increased with aging time up to peak hardness condition. Further aging above peak hardness resulted in decrease in conductivity which proved the over-aging of the structure. Moreover, in most cases the multi-step precipitation sequence can be easily

detected by monitoring various steps in electrical conductivity values. Hence, it was demonstrated that a good correlation exists between progress of aging and electrical conductivity.

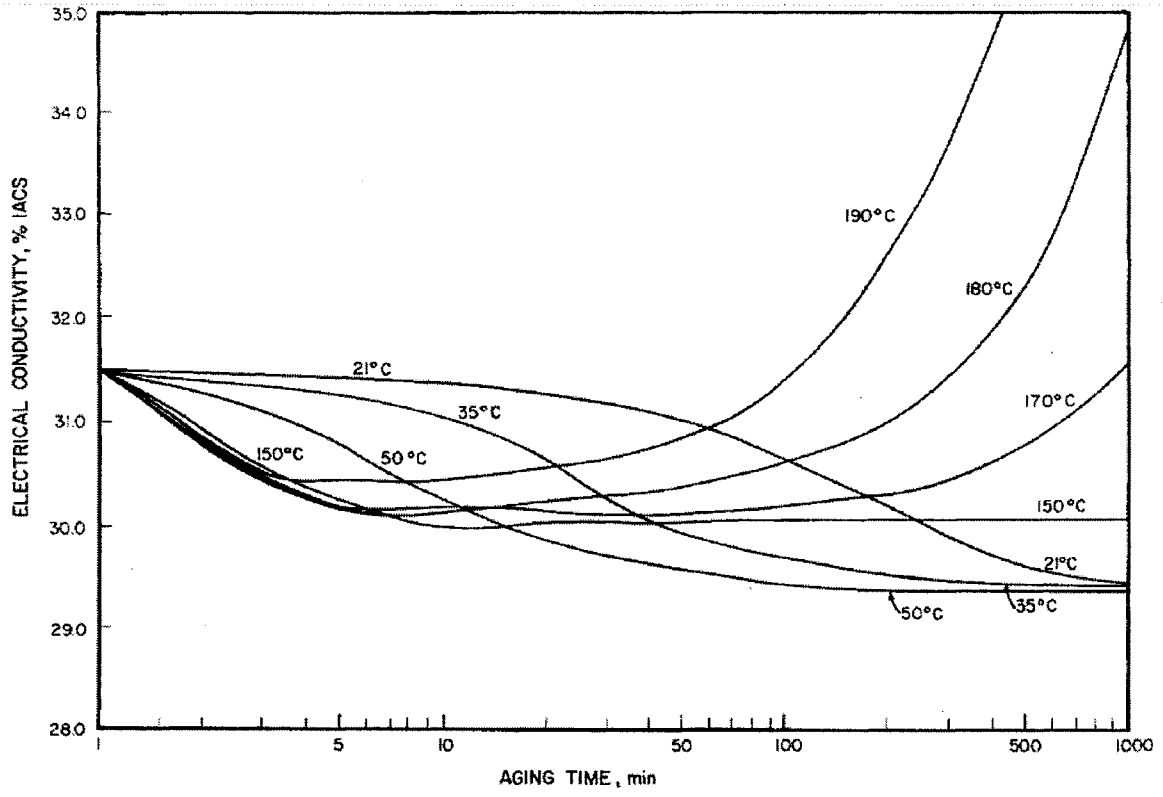

Figure 2.11 Eddy current conductivity *vs.* aging time in unstretched samples of aluminum alloy 2024 [47]. The conductivity is corrected to 20 °C.

Lee *et al.* [52] and Salazar-Guapuriche *et al.* [53] both observed that the hardness values versus electrical conductivity plots yield C-shaped plots. The overall relationship

between hardness and electrical conductivity is not linear. Salazar-Guapuriche *et al.* [53] also found that in the natural and over ageing conditions, electrical conductivity and hardness showed a reciprocal effect, i.e. an increase in one produced a decrease in the other and vice versa, as shown in Figure 2.12. During natural aging process, hardness increases because of precipitation hardening while the electrical conductivity decreases. In over aging condition, hardness decreases due to the growth of precipitates while the electrical conductivity continues increasing.

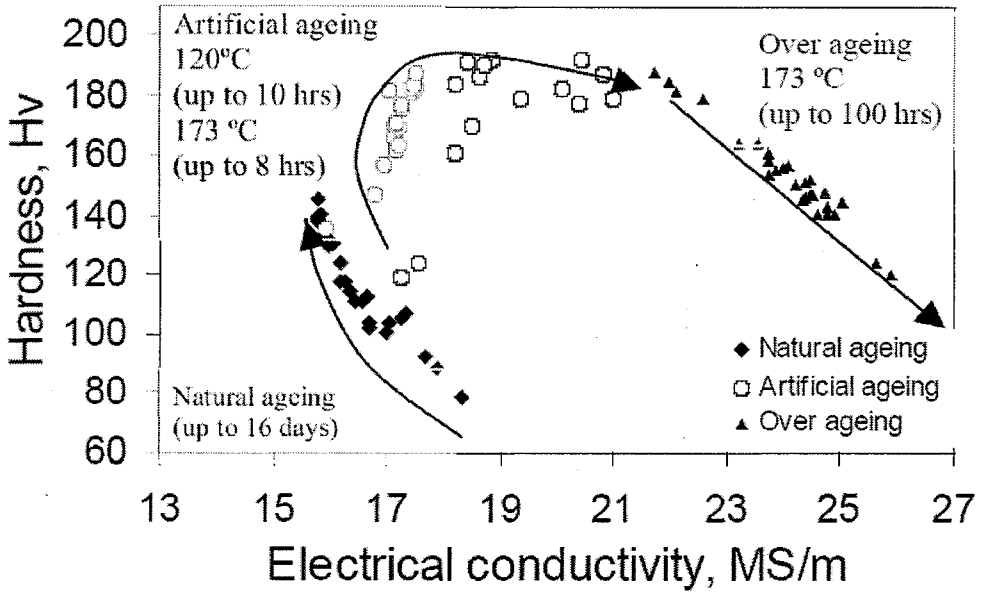

Figure 2.12 Hardness and electrical conductivity profile ofAA7010 at different stages of ageing treatment. The progress of ageing with temperature and time is indicated [53].

3 EXPERIMENTAL PROCEDURES

3.1 Materials

The AA2618 aluminum alloy studied was received from PCP Canada Ltd. in the form of a cross-section slice (54 in × 16 in × 2 in) cut directly from a large AA2618 DC cast ingot. The chemical composition of the alloy is listed in Table 3.1.

Table 3.1 Chemical composition (wt %) of the AA2618 alloy.

Cu	Mg	Fe	Ni	Si	Zn	Ti	Mn	Al
2.86	0.97	0.97	1.04	0.14	0.10	0.02	<0.01	Bal.

The mechanical properties of the surface and center parts of the cast plate usually have variations due to the chemical segregation and the different cooling rates during casting process. Therefore, surface and center samples measuring 2.5 in × 1.5 in × 1.0 in were cut, respectively, from the AA2618 cast plates for heat treatment and hardness testing. The positions of the samples are shown in Figure 3.1.

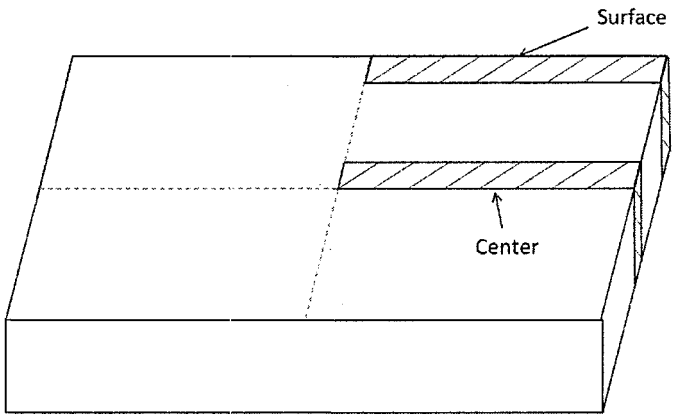

Figure 3.1 Schematic graph indicating the positions of samples on the cross-section of the ingot.

3.2 Heat Treatments

The heat treatments proposed were carried out at various temperatures for different holding times in the forced-air electric furnace shown in Figure 3.2. The heat treatment procedures will be discussed in the following subsections.

Figure 3.2 Forced-air electric furnace.

3.2.1 Solution Heat Treatment and Quenching

The solution treatment conditions shown in Table 3.2 were divided into three groups according to the solution treatment parameters studied, namely solution temperature, holding time, and quenching medium. The schematic drawing shown in Figure 3.3 describes the sequence of the solution treatments applied. All samples were further aged at 200 °C for 20 h.

Table 3.2 Solution treatment conditions applied to AA2618 samples.

Group	Solution treatment parameters		
	Temperature (°C)	Holding time (h)	Cooling method
I*	480, 505, 530 and 545	5	Water Quenching (WQ)
II*	480, 505, 530 and 545	5	Air Cooling
III*	530	1, 3, 5, 8, and 12	Water Quenching (WQ)

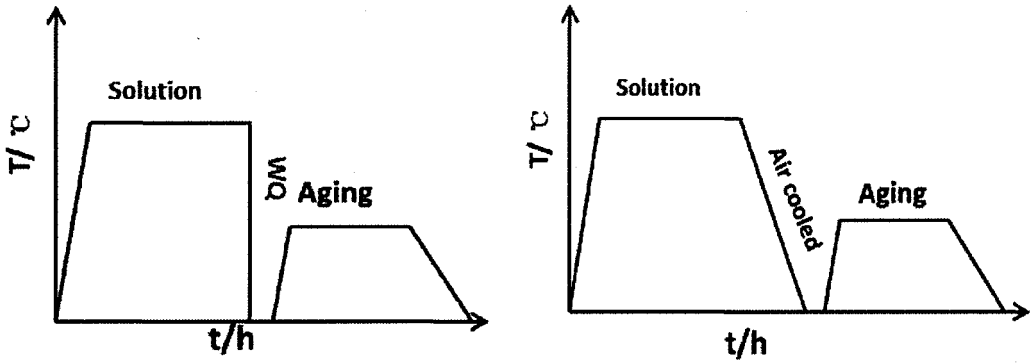

Group I and III

Group II

Figure 3.3 Schematic graphs showing the solution treatment sequences.

3.2.2 Artificial and Natural Aging

Samples prepared for aging treatment investigations were first solution treated at 530 °C for 5 h followed by water quenching. They were subsequently grouped and aged at room temperature, 175, 195 and 215 °C, respectively, for different holding times ranging from 1 h to 5 weeks. After aging, the samples were air cooled to room temperature.

3.3 Metallographic Microstructure Examination

For metallographic observations, 10×10 mm samples were cut from the as-cast and solution-treated alloy samples and mounted in bakelite using a Struers Labopress-3 Mounting Press shown in Figure 3.4. The samples were then ground and polished to the desired fine finish by means of a Struers Tegrapol-35 Grinder-Polisher, see Figure 3.5. The grinding was carried out using successively #120, # 240, # 320, # 500, # 800 grit SiC papers. The polishing was carried out by applying polycrystalline diamond powder suspended in water with particles of 6 μm and 3 μm for rough and fine polishing, respectively. Struers oil is used in both polishing stages as a cooling and lubricating medium. Finally, to produce a mirror-like surface of the samples, the ultimate polishing stage was completed using 1 μm colloidal silica suspension with water as a coolant and

lubricant. After polishing, the mounted samples were washed with a mix of soap and alcohol, and then dried using compressed air. The samples used for identification of Al_9FeNi phase were etched for 5 s at ambient temperature in etchant solution with chemical composition of 1 ml HF(40%), 3 ml HCl(38%), 5 ml HNO3(70%) and 191 ml distilled water.

Figure 3.4 Struers Labopress-3 Mounting Press.

Figure 3.5 Struers Tegrapol-35 Grinder-Polisher.

The microstructures were examined by means of a Nikon Eclipse SE600 optical microscope (Figure 3.6). Phase identification was carried out using a JEOL JSM-6480LV Scanning Electron Microscope (SEM), shown in Figure 3.7, in conjunction with energy dispersive X-ray spectrometer (EDS) operated at 20KV.

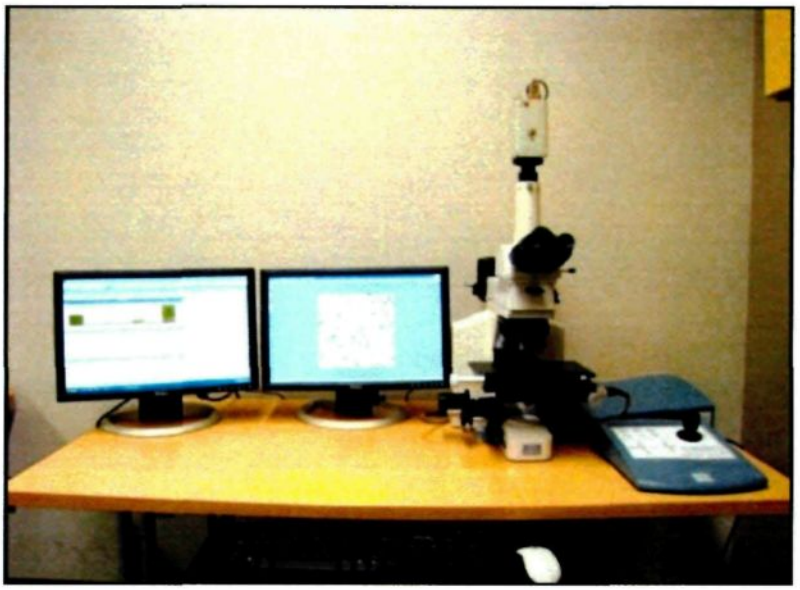

Figure 3.6 Nikon Eclipse SE600 optical microscope.

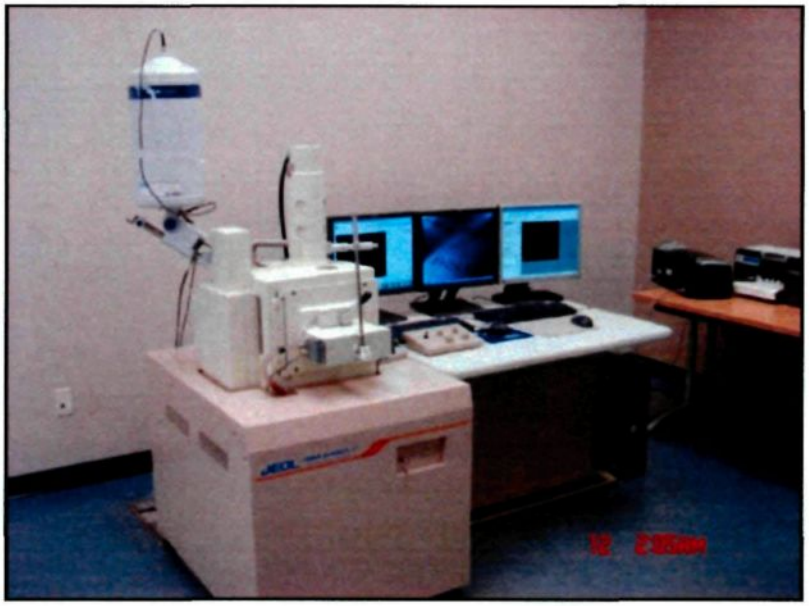

Figure 3.7 JEOL JSM-6480LV scanning electron microscope.

3.4 DSC Analysis

DSC analysis was carried out on various as-cast and heat-treated samples using a

computerized PerkinElmer DSC8000 differential scanning calorimeter shown in Figure 3.8. The weight of the DSC samples was approximately 20 mg and the heating/cooling rate was fixed at 10 °C/min. A protective gas atmosphere of pure argon was applied.

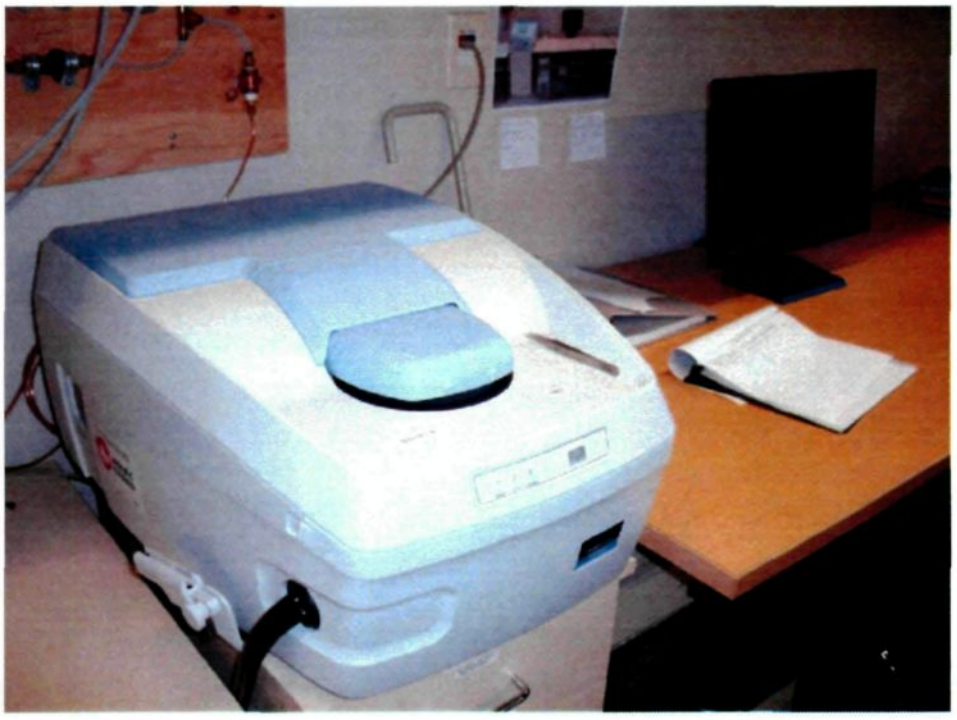

Figure 3.8 PerkinElmer DSC8000 differential scanning calorimeter.

As-cast samples were analyzed by DSC to determine the melting points of the intermetallic phases involved in the AA2618 alloy studied. This makes it possible to find out the optimum solution treatment temperature for the alloy. Samples after solution treatment and aging were also analyzed by DSC in order to investigate the impact of

solution treatment on the dissolution of the intermetallic phases and to detect the phases responsible for the precipitation hardening process.

3.5 Hardness Test

The hardness measurements were conducted on all the samples using a QualiRock Rockwell Hardness Tester shown in Figure 3.9. The tester is equipped with a steel ball indenter with a diameter of 1/16 in. The indenter was first manually pressed into the sample to a certain degree by a minor load of 10 kgf and the zero datum was established. A major load of 50 kgf was then applied for a dwell time of 3 s. The resulting Rockwell number, scale F, represents the difference in depth from the zero datum position as a result of the application of the major load.

Figure 3.9 Rockwell hardness tester.

3.6 Tensile Test

The tensile properties, namely yield strength (YS) at a 0.2% offset strain, ultimate tensile strength (UTS), and fracture elongation (%El), were tested for selected conditions at room temperature using an Instron-3382 universal testing machine shown in Figure 3.10 at a constant strain rate of 2.7×10^{-2} s^{-1}. The dimensions of the tensile sample used

are shown in Figure 3.11. The tensile properties of each condition are the average values of 4 test samples.

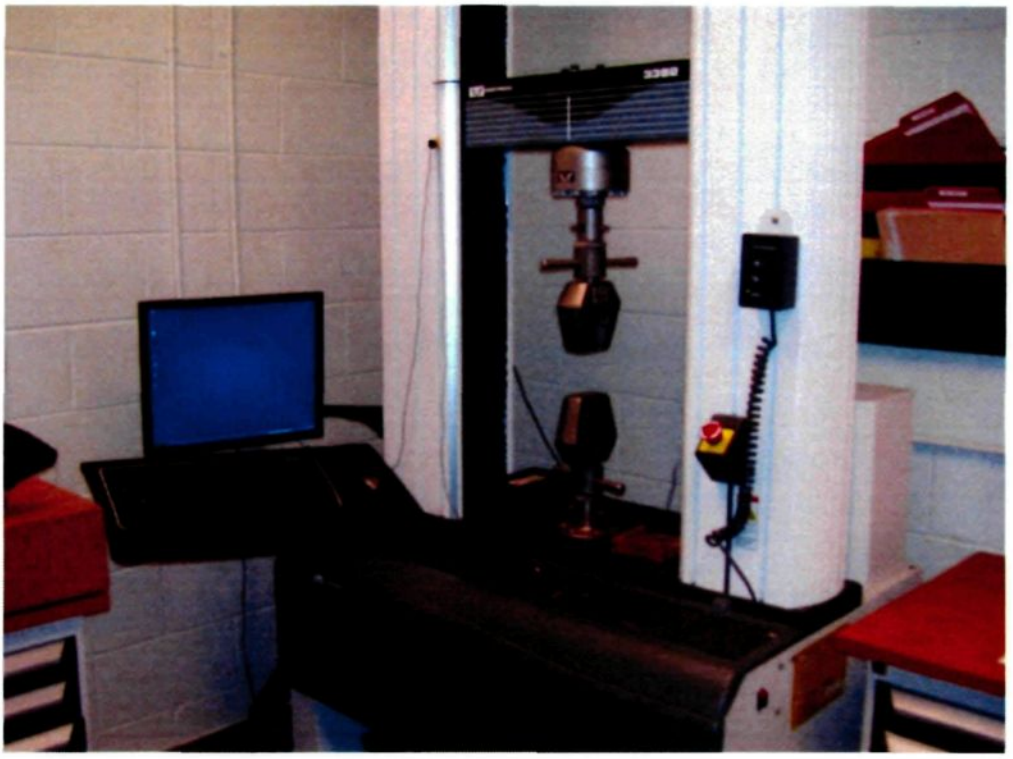

Figure 3.10 Instron-3382 universal tensile testing machine.

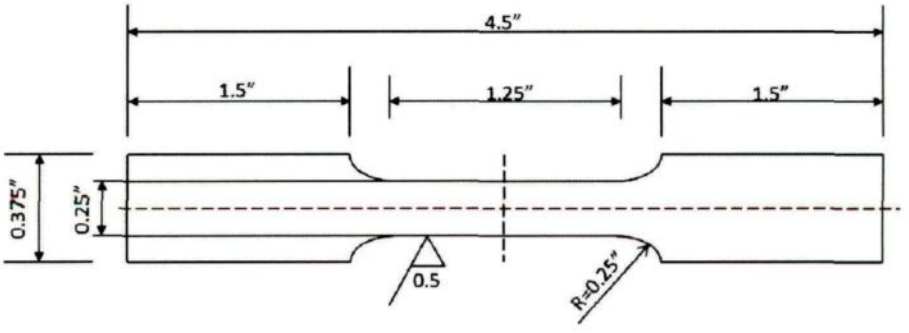

Figure 3.11 The dimensions of the tensile sample.

3.7 Electrical Conductivity Measurement

Eddy current testing technique was used for measuring the electrical conductivity of the AA2618 alloy in all heat-treated conditions. Electrical conductivity was measured on ground and polished samples in accordance with ASTM standard E 1004-94 using portable FISCHER SIGMASCOPE®SMP 10 Electrical Conductivity Measurement System shown in Figure 3.12. An electrical conductivity measurement probe with a diameter of 11 mm was used for all measurements. The change in the electrical conductivity was measured at room temperature in terms of percentage of international annealed copper standard (%IACS). Before conducting electrical conductivity test, the equipment was calibrated on standards of known conductivity. The measured values were considered to be accurate within ±0.5 %IACS. Six readings were taken for each sample and then the average value was calculated for plotting the graph of electrical conductivity verses aging time.

Figure 3.12 FISCHER SMP 10 Electrical Conductivity Measurement System.

3.8 Quench Sensitivity Test

AA2618 alloy plates were machined into cylindrical bars which would be used for the quench sensitivity test. The bars were 35 mm in diameter and 160 mm long. They were surrounded by insulating asbestos except the two ends in order to create a one-dimensional heat transfer environment along the axial direction of the bar. By this way, the heat transfer along the sides of the cylinder would not occur and the radial variation of hardness could be avoided. Small holes were drilled in the bars at different distances measured from the quench ends to introduce up to seven type K thermocouples that were connected to a PC-based data logging system, as shown in Figure 3.13, to

record temperature changes during heating and cooling.

The bars were solutionized for 5 h at 530 °C in the forced-air electric furnace shown in Figure 3.2. The furnace door was then opened and the test bar was grabbed using insulated gloved hands. The bar was placed on the Jominy end quench fixture as shown in Figure 3.14 and the water flow to the nozzle was initiated. The time elapsed between the opening of the furnace door and the initiation of water flow was approximately 5 s. Once the temperature of the whole bar dropped to below 50 °C, the bar was removed from the fixture and immediately placed into a room temperature water bath. After reaching room temperature, the bar was dried and then aged at 215 °C for 1 h.

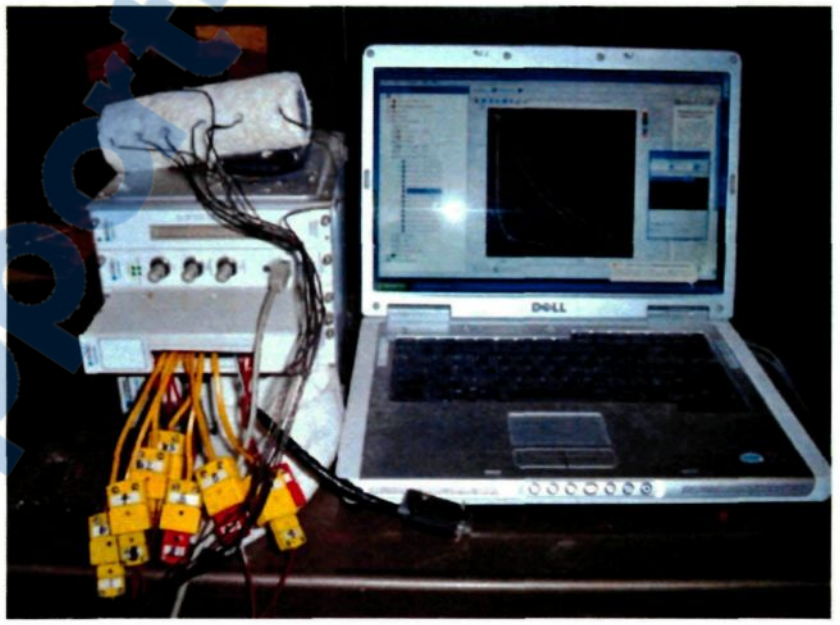

Figure 3.13 Insulated cylindrical bar and PC-based data logging system.

Figure 3.14 Jominy end quench fixture.

After aging, the quench test bars were sliced at the distances corresponding to the positions of thermocouples. Hardness test was carried out on the cross sectional areas of the resulting slices using Rockwell F scale. Hardness profiles of AA2618 aluminum Jominy end quench bars could be plotted versus cooling rate with the intention of determining the quench sensitivity of AA2618 aluminum alloy.

4 RESULTS AND DISCUSSION

4.1 Characterization of the As-cast Microstructure of the AA2618 Alloy

The as-cast microstructure of the received AA2618 aluminum alloy was first investigated in order to identify the intermetallic phases contained as a basis for the following research work.

4.1.1 Metallographic Observations

The optical micrograph shown in Figure 4.1 (a) reveals that the as-cast structure of the AA2618 alloy consists of uniform equiaxed α-Al grains along with a considerably high amount of coarse intermetallic phases distributed at the aluminum dendrite boundaries. At higher magnification (Figure 4.1 (b)), three different intermetallic phases, namely block-like Al_2Cu, branched Al_9FeNi, and trace dark Mg_2Si, can be clearly observed. The optical micrograph shown in Figure 4.2 was obtained from as-cast AA2618 alloy sample after etching, in which the Al_9FeNi phase can be obviously identified in brown color. The Al_9FeNi phase, which exists as block-like or branched

particles, is the predominant intermetallic phase in the alloy microstructure.

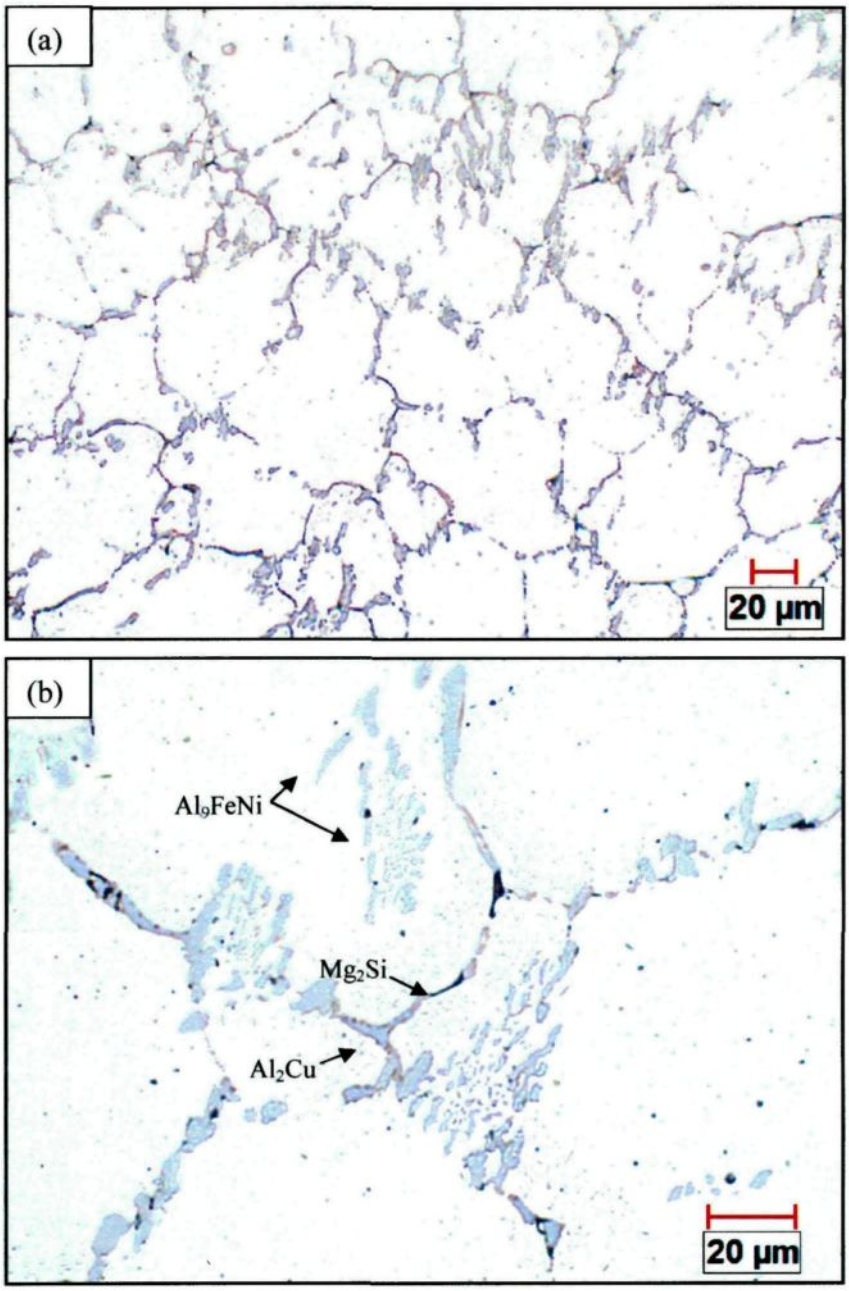

Figure 4.1 Optical micrographs showing the as-cast microstructure of the AA2618 alloy at: (a) low magnification (200×); and (b) high magnification (500×).

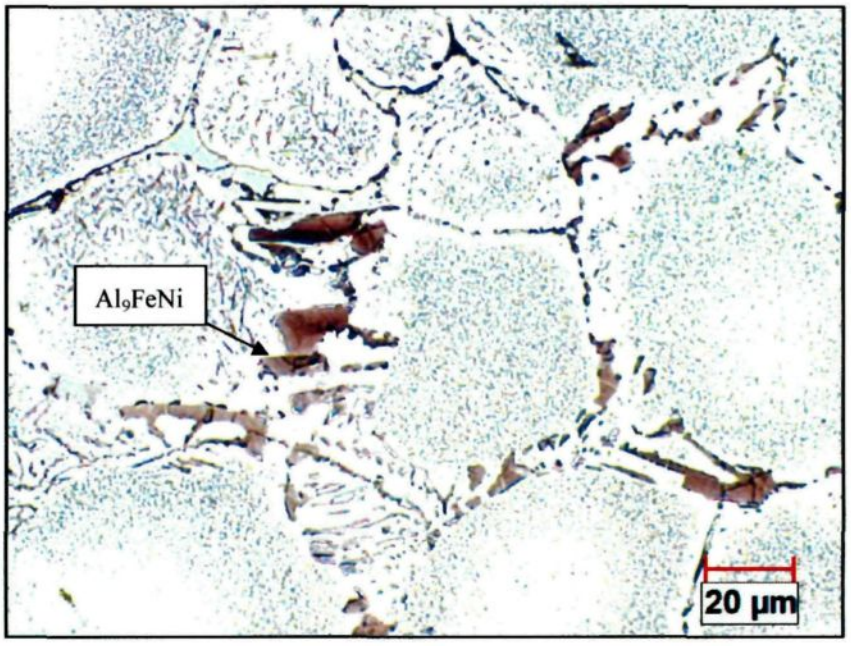

Figure 4.2 Optical micrograph obtained from as-cast 2618 aluminum alloy sample after etching.

The higher magnification backscattered electron (BSE) images shown in Figure 4.3 display all the intermetallic phases contained in the as-cast AA2618 alloy microstructure with different features. The bright phases, 2 and 3, might contain Cu, which has a higher atomic number and consequently can backscatter more electrons to make the phases seem brighter in the BSE images. On the contrary, the dark phases, 1 and 5, might contain Fe, which has a lower atomic number making the Fe-containing phases appear darker.

Based on the Energy Dispersive X-Ray (EDX) Analysis results shown in Figure 4.4,

the dark gray branched or irregular phase (labeled 1) can be determined approximately as Al_9FeNi phase, which was found to be the predominant intermetallic phase in the alloy microstructure. The bright elongated phase (labeled 2) contains Al, Cu and Ni as major elements and may be considered as Al_7Cu_4Ni phase. The bright round phase (labeled 3) and the lamellar eutectic structure (labeled 4) can be identified as Al_2Cu phase and Al/Al_2CuMg eutectic phase, respectively. The gray needle-like phase labelled 5 in Figure 4.4 (b) contains Al, Cu, Fe and Ni and the ratio of Cu to the sum of the Fe and Ni contents is approximately 2:1, and therefore can be designated as $Al_7Cu_2(Fe,Ni)$ phase.

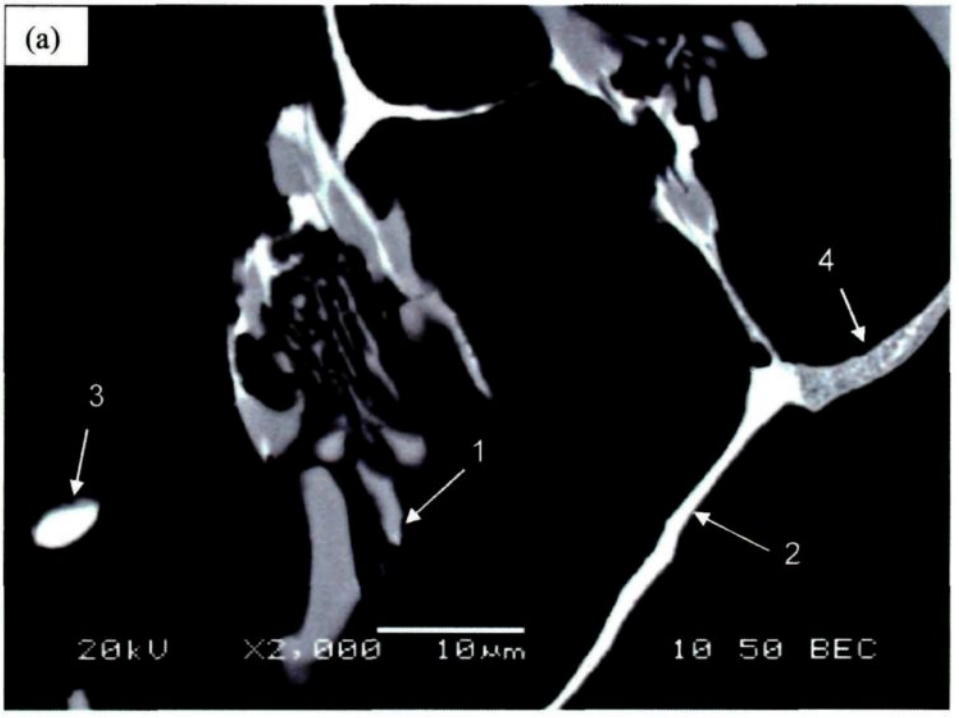

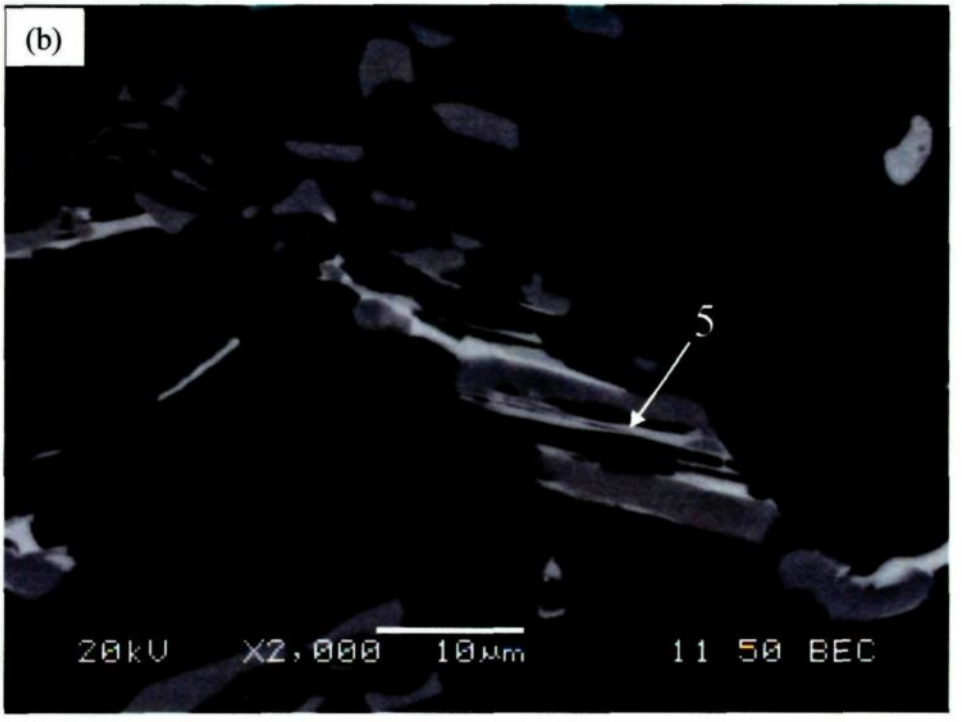

Figure 4.3 Backscattered electron (BSE) images obtained from as-cast AA2618 sample.

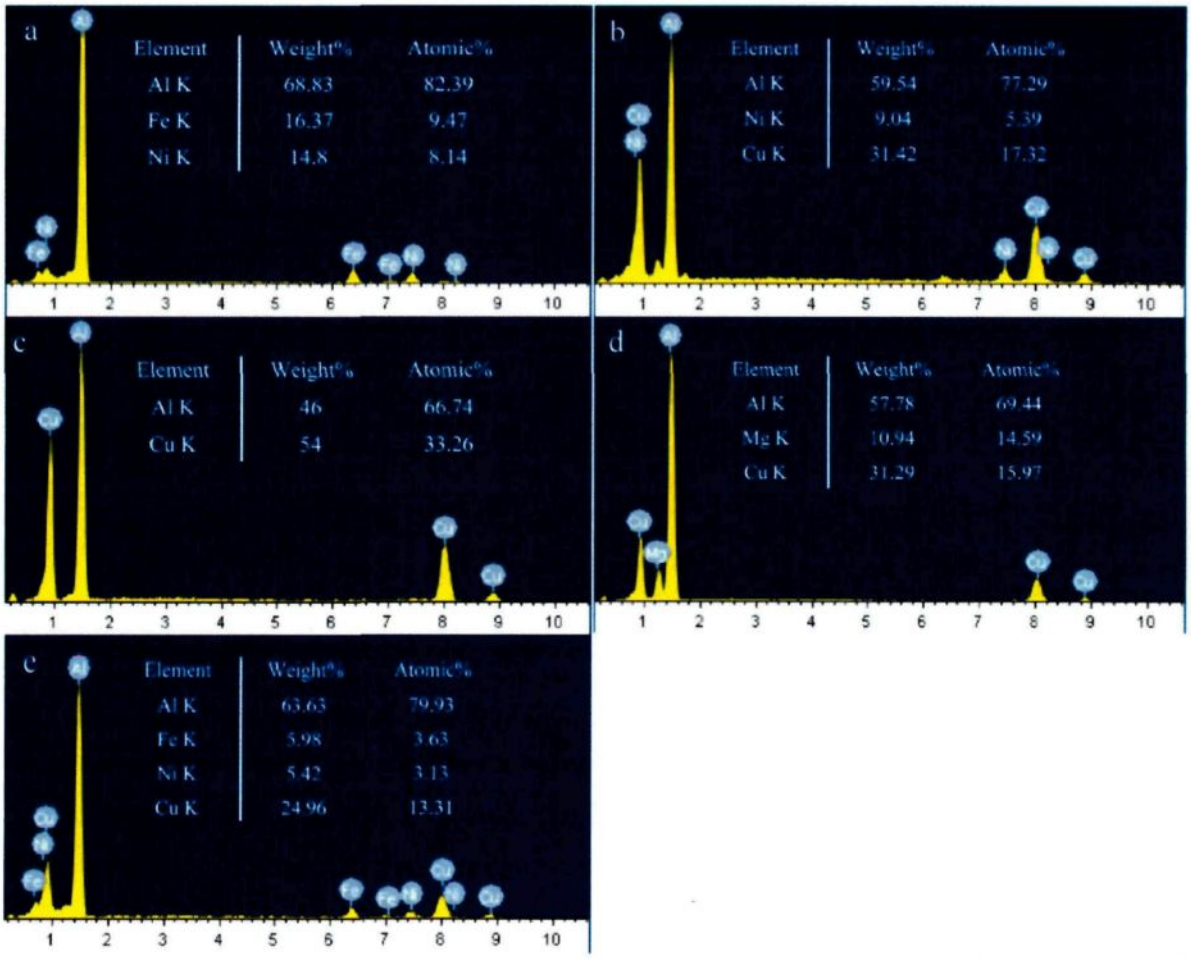

Figure 4.4 EDX spectra corresponding to the intermetallic phases shown in Figure 4.3: (a) Al_9FeNi (labeled 1), (b) Al_7Cu_4Ni (labeled 2), (c) Al_2Cu (labeled 3), (d) Al_2CuMg (labeled 4), and (e) $Al_7Cu_2(Fe,Ni)$ (labeled 5).

4.1.2 DSC Analysis

DSC analysis was used to determine the melting points of the intermetallic phases formed in the as-cast AA2618 alloy with the intension of optimizing the solution

treatment of the alloy. Figure 4.5 shows the relevant DSC curve, which exhibits six endothermic peaks at 508.3, 539.9, 553.4, 575.5, 634.0 and 636.5 °C. The first peak represents the low melting point of the eutectic like Al_2CuMg phase precipitated by a quaternary eutectic reaction at the last stage of solidification. The second peak is attributed to the melting of block-like Al_2Cu phase. The following three peaks may be related to the melting of intermetallic phases, namely Al_7Cu_4Ni, $Al_7Cu_2(Fe,Ni)$ and Al_9FeNi, respectively. The last large peak corresponds to the bulk melting of the primary α-Al.

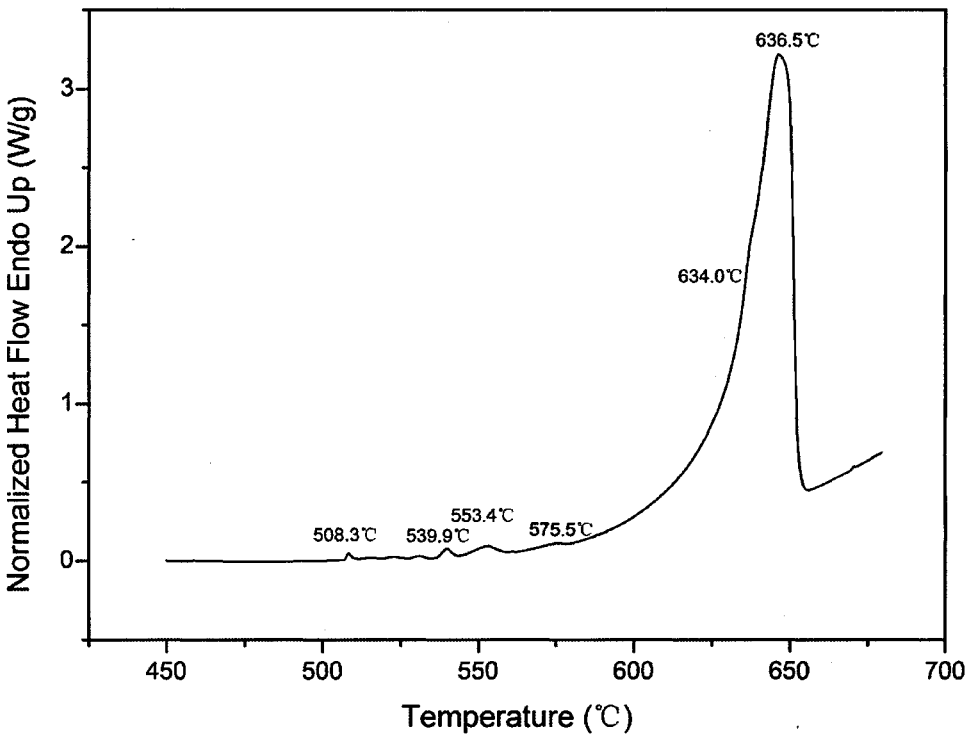

Figure 4.5 DSC heating curve of as-cast AA2618 alloy.

4.2 Effects of Solution Treatment

4.2.1 Metallographic Observations

The BSE images shown in Figure 4.6 (a-d) display the microstructure of the AA2618 alloy after solution treatment for 5 h at different temperatures ranging from 480 °C to 545 °C. It can be observed that as the solution treatment temperature increases from 480 °C to 545 °C, the intermetallic phases undergo a pronounced change when compared to the as-cast microstructure shown in Figure 4.1 and 4.3. Solution treatment whether at 480 °C or 505 °C can partially dissolve the bright Cu-containing phases, namely Al_2Cu, Al_2CuMg and Al_7Cu_4Ni, as shown in Figure 4.6 (a-b). After solution treatment at 530 °C, these phases seem to become almost completely dissolved in the solid solution. The gray Al_9FeNi phase was only subjected to partial fragmentation and spheroidization, particularly at 530 and 545 °C.

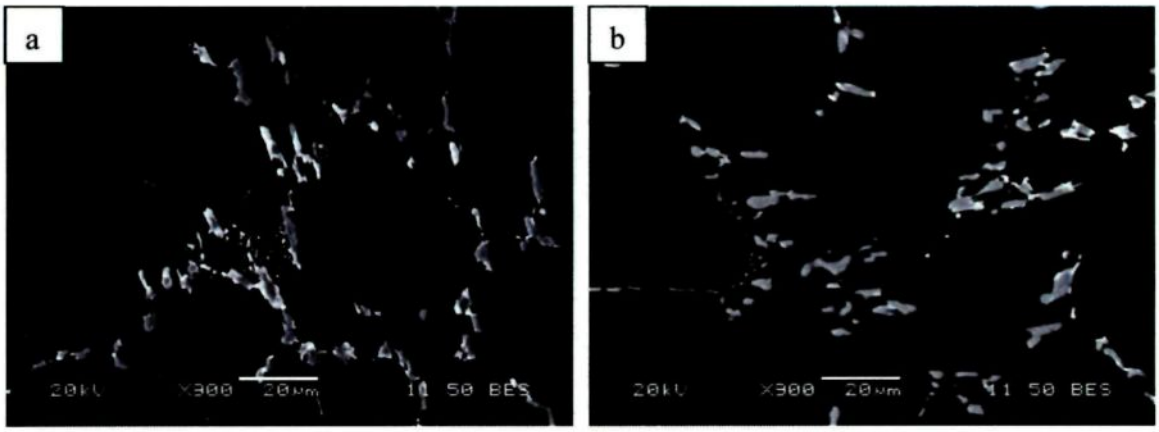

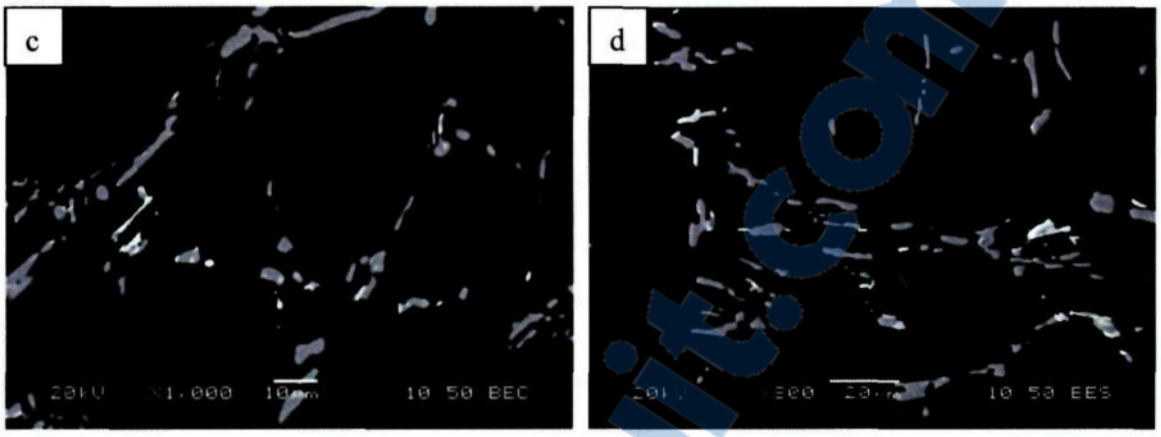

Figure 4.6 BSE images of AA2618 alloy samples solution treated for 5 h at various temperatures: (a) 480 °C, (b) 505 °C, (c) 530 °C, and (d) 545 °C.

In order to understand the evolution of the intermetallic phases during the solution treatments, higher magnification BSE images were captured and the EDX analysis was applied to analyze the chemical composition. Figure 4.7 shows the BSE image of an AA2618 alloy sample solution treated at 480 °C for 5 h. The EDX analysis results of the phases labeled in this image are provided in Table 4.1. It can be found that some Al_7Cu_4Ni phase particles were subjected to a fragmentation while the ratio of Cu to Ni changed from 4:1 to 1:1, which implies that the Al_7Cu_4Ni phase was transformed during the solution treatment to a new phase (labeled b) with a formula of Al_7CuNi. The Al_9FeNi and $Al_7Cu_2(Fe,Ni)$ phases (labeled a and c, respectively) were not obviously affected by the solution treatment at 480 °C for 5 h.

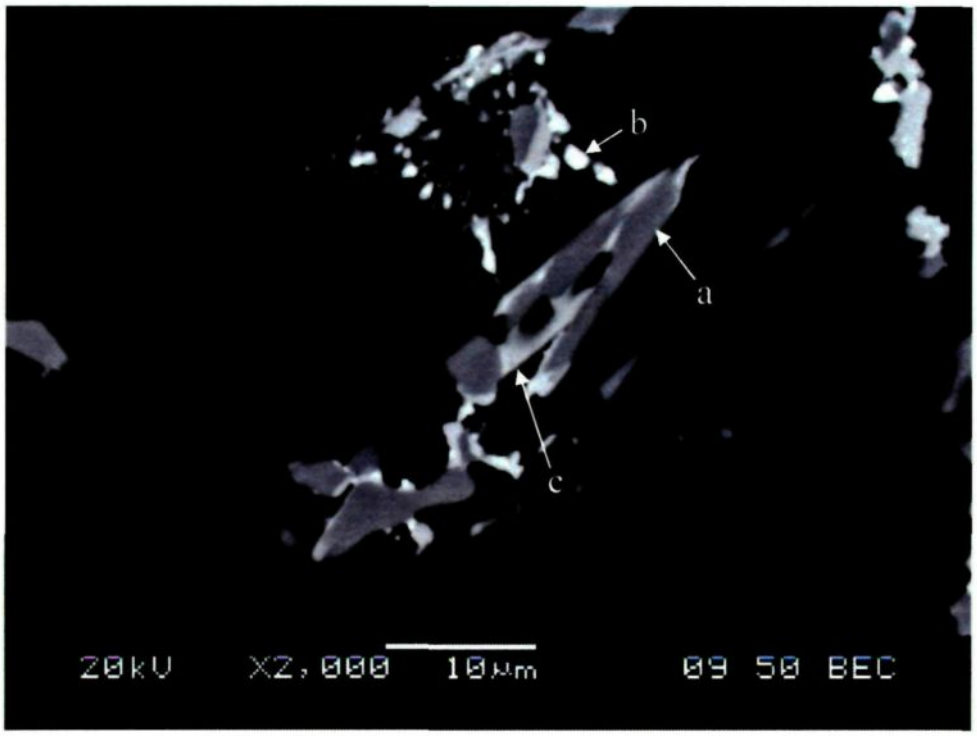

Figure 4.7 Higher magnification BSE image of AA2618 sample solution treated at 480 °C for 5 h.

Table 4.1 SEM-EDX spectrum analysis of the phases labeled in Figure 4.7 (at. %).

Phase	Al	Fe	Ni	Cu	Formula of phases
a	86.42	7.34	6.24	—	Al_9FeNi
b	77.20	—	10.03	12.77	Al_7CuNi
c	78.51	3.68	4.09	13.72	$Al_7Cu_2(Fe,Ni)$

The transformation of the Al_7Cu_4Ni phase into the Al_7CuNi phase also occurred after solution treatment at 505 °C, as can be discerned from Figure 4.8. It is worth noting from Figure 4.9 and Figure 4.10 that after solution treatments at 530 and 545 °C the

Al_7CuNi phase cannot be observed any more, which indicates that this phase has been completely dissolved. This observation is in contrary with the work of Feng *et al.* [11] and Wang *et al.* [12] in which they concluded that no obvious change was observed on the size and morphology of the Fe or Ni containing compounds. The dissolution of Al_7CuNi phases at higher solution temperature would improve the precipitation hardening effect during aging treatment to a large extent by contributing more Cu atoms into the supersaturated α-Al solid solution. The remaining Al_9FeNi and $Al_7Cu_2(Fe,Ni)$ phase particles have no obvious composition change. They have been only subjected to fragmentation and spheroidization.

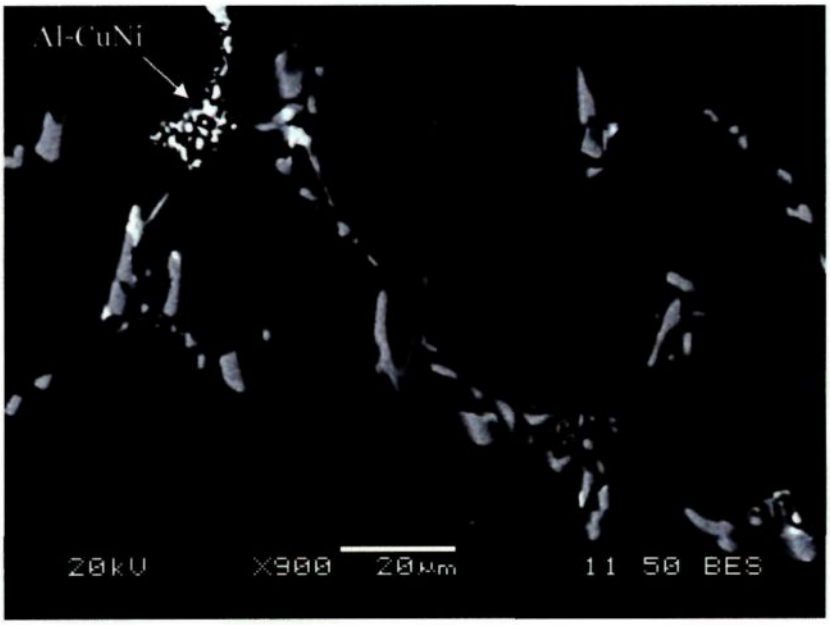

Figure 4.8 Higher magnification BSE images of AA2618 sample solution treated at 505 °C for 5 h.

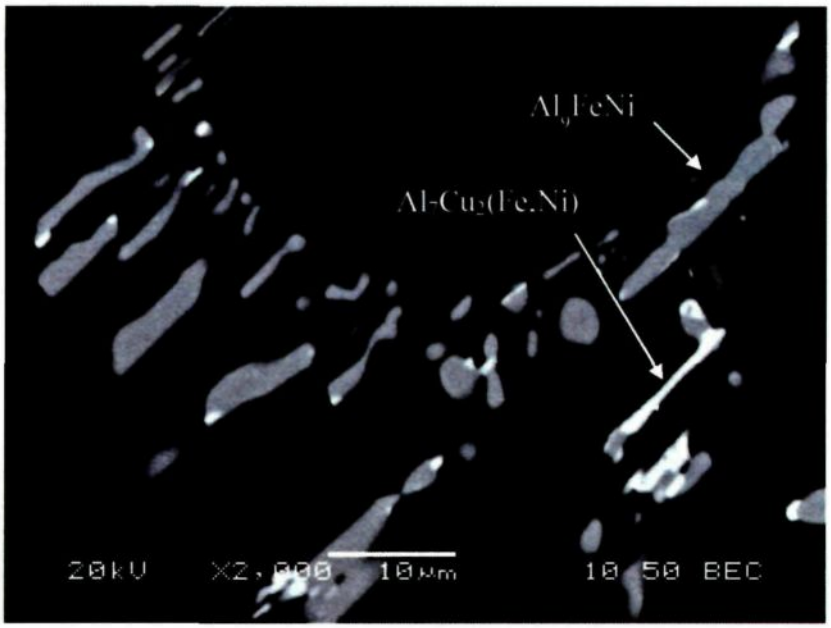

Figure 4.9 Higher magnification BSE images of AA2618 sample solution treated at 530 °C for 5 h.

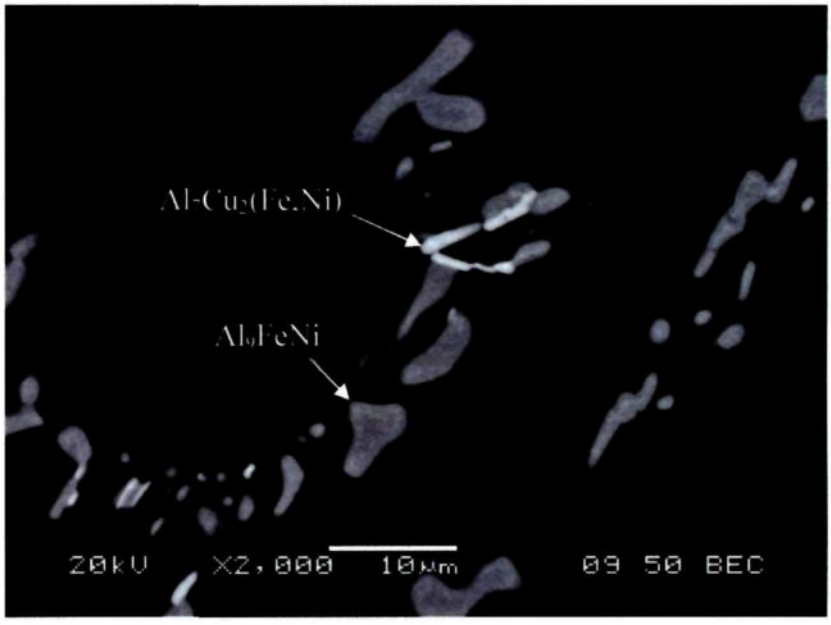

Figure 4.10 Higher magnification BSE images of AA2618 sample solution treated at 545 °C for 5 h.

Slight overheating happened in the AA2618 alloy at solution temperature of 545 °C, as shown in Figure 4.11. Low melting point eutectics were melted near the grain boundaries forming a hard and persistent spherical structure (marked A) which will act as a potential crack source and consequently decreases the mechanical properties [6]. Therefore, the overheating temperature of the AA2618 alloy can be specified to be 545 °C, whereas the optimum solution treatment temperature is 530 °C. In the practical industrial applications, the solution temperature should be precisely controlled to keep the low melting point copper-rich phases away from the detrimental incipient melting, while dissolving the greatest amount of such phases into the Al matrix.

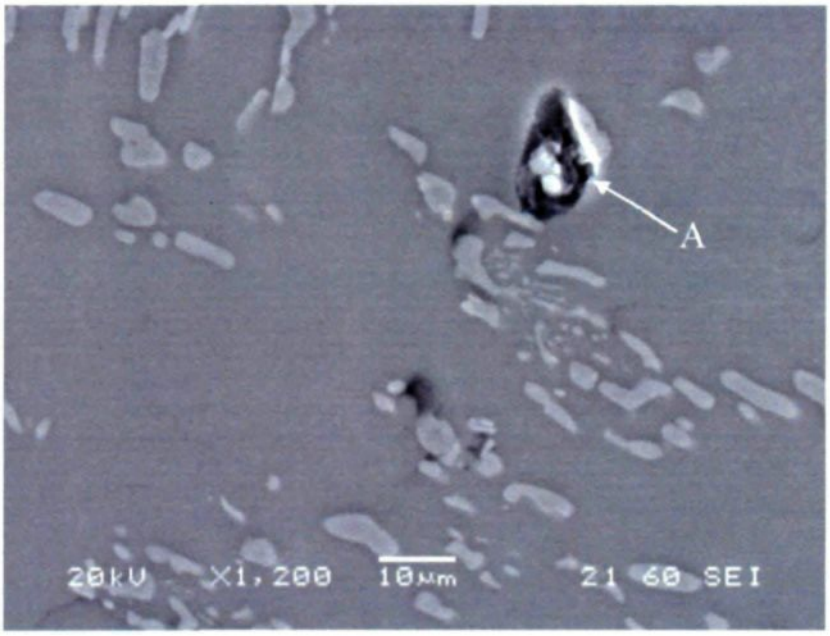

Figure 4.11 Secondary electron image showing slight overheating in AA2618 alloy sample solution treated at 545 °C for 5h.

Figure 4.12 shows the BSE images of AA2618 alloy samples solution treated at 530 °C for different soaking times ranging from 1 to 12 h. The remarkable changes caused in the microstructure can be observed after 1 h solution treatment where a large amount of the bright Cu-containing phases were dissolved into the solid solution and the Al_9FeNi phase was fragmented into smaller discontinuous phase particles. After 5 h solution treatment, the low melting point Cu-rich phases seem to be fully dissolved into the Al matrix. The bright phase remained in the matrix was identified as $Al_7Cu_2(Fe,Ni)$ phase, as mentioned above. Prolonged solution treatment at 530 °C for 8 h and 12 h did not bring any further significant changes in the microstructure as compared to solution treatment for less time.

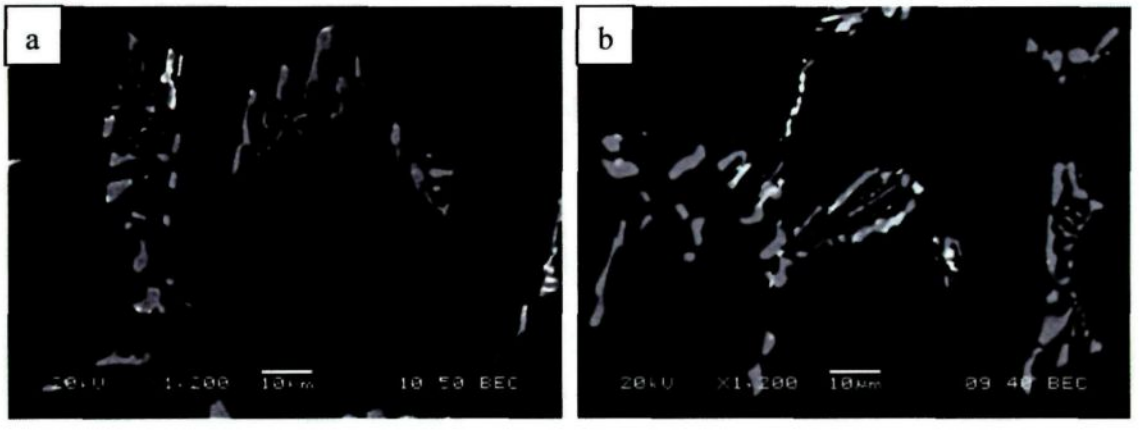

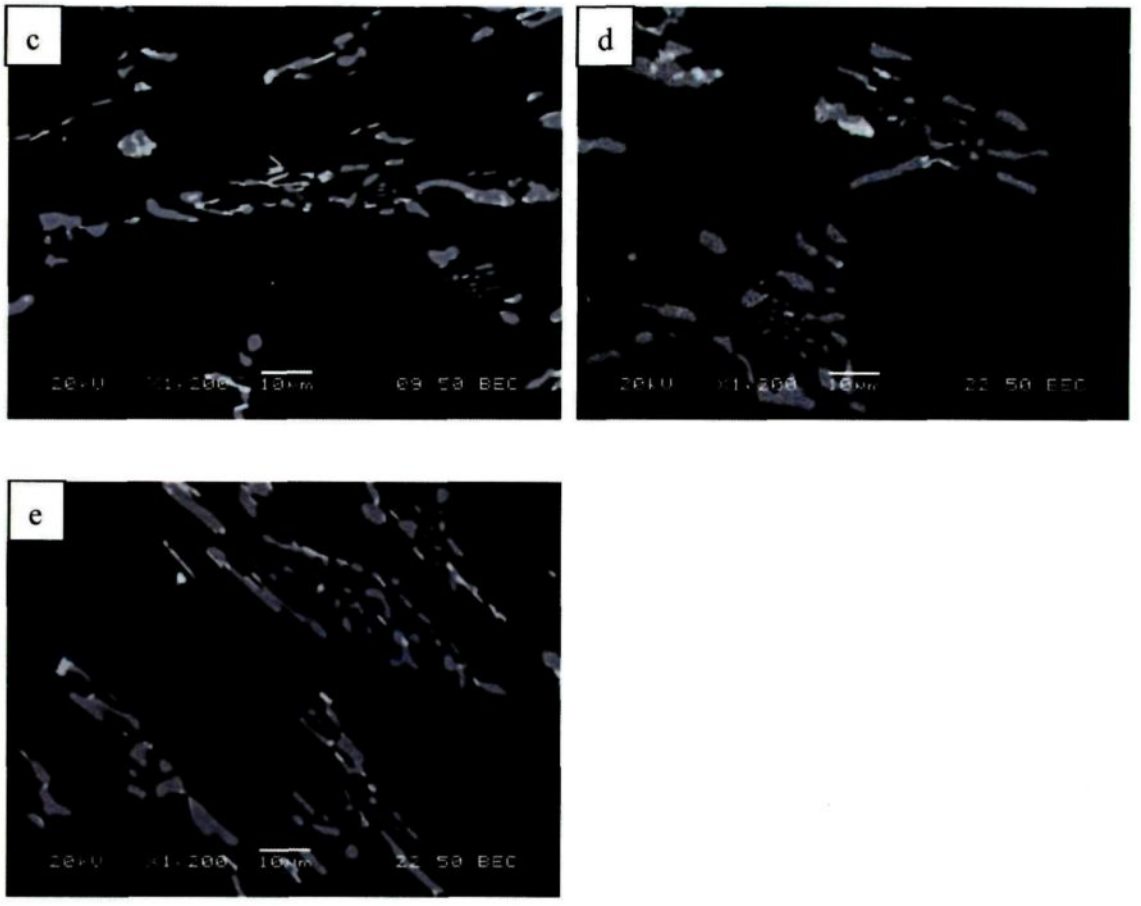

Figure 4.12 BSE micrographs of AA2618 samples solution treated at 530 °C for varied times: (a) 1 h; (b) 3 h; (c) 5 h; (d) 8 h; (e) 12 h.

4.2.2 DSC Analysis

Figure 4.13 shows the DSC heating curves of the AA2618 alloy after solution treatment for 5 h at different temperatures. After solution treatment at 480 °C, the first peak disappeared, whereas the height of the second peak has no obvious change. This

implies that solution treatment at 480 °C for 5 h could dissolve Al_2CuMg phase entirely into the solid solution and has no significant impact on the Al_2Cu phases. Solution treatment at 505 °C leads to the disappearance of the endothermic peak corresponding to the melting of Al_2Cu phase. This observation indicates that solution treatment at 505 °C for 5 h is successful in dissolving the Al_2Cu phase completely into the solid solution.

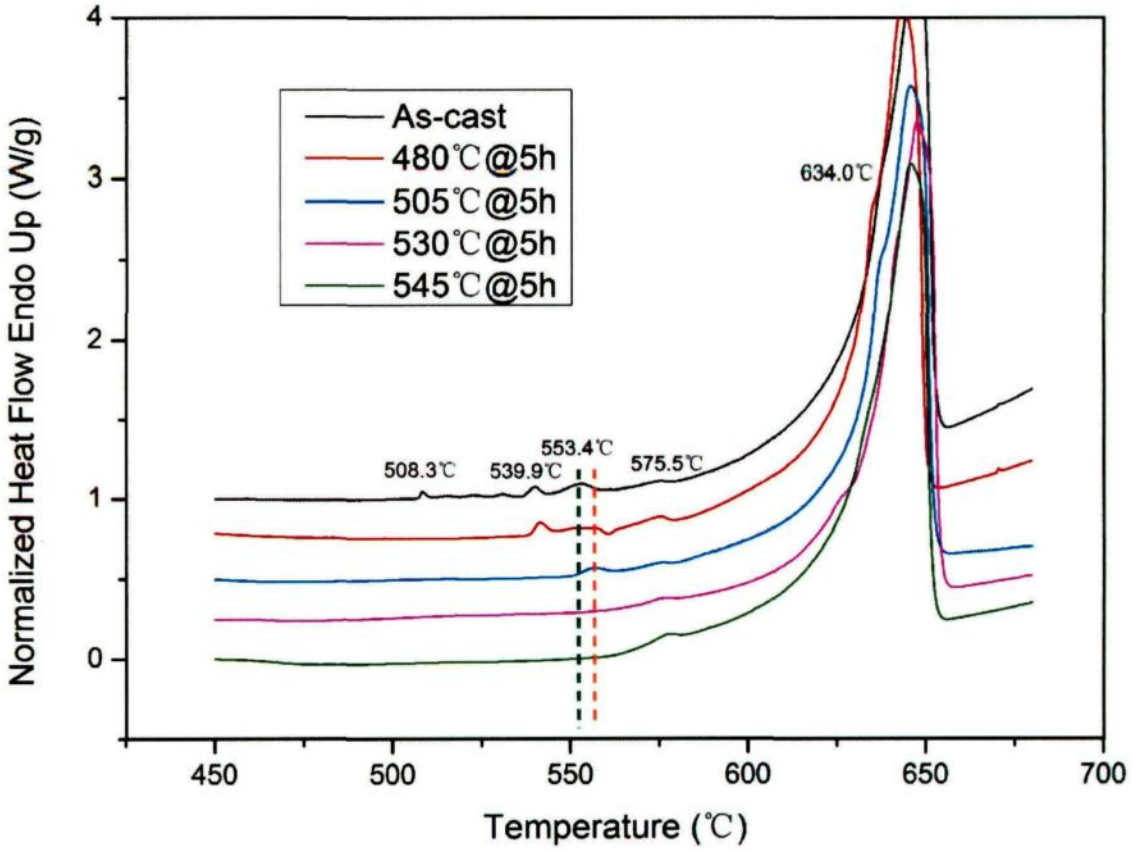

Figure 4.13 DSC heating curves of AA2618 samples solutionized for 5 h at different temperatures

The intermetallic phases containing Fe or Ni, which melt at higher temperatures as represented by the subsequent peaks, were not significantly affected by the solution treatment whether at 480 or 505 °C. The only change that can be observed after these solution treatments is a slightly right shift occurred in the endothermic peak, corresponding to the melting of the Al_7Cu_4Ni phase from 553.4 °C (green dashed line) to 556.0 °C (orange dashed line), which indicates that the composition of this phase might be changed by the solution treatment. This result is consistent with the preceding microstructure observation, which revealed the transformation of the Al_7Cu_4Ni phase into the Al_7CuNi phases. With the increase of solution temperature, the endothermic peak corresponding to the melting of the Al_7CuNi phase disappeared, which indicates that this phase was completely dissolved by the solution treatment at higher temperature. As a result, the Al matrix has become enriched by Cu element, which would contribute to the following precipitation hardening effect and promote the mechanical properties of AA2618 alloy.

Solution treatments at higher temperatures 530 and 545 °C did not, however, affect the $Al_7Cu_2(Fe,Ni)$ and Al_9FeNi phases as can be manifested by the presence of their endothermic peaks at 575.5 and 634.0 °C, respectively, on the DSC curves corresponding to these solution temperatures. It is obvious that all these results obtained from the DSC

analysis are in line with the preceding microstructure observations.

The DSC heating curves of samples solutionized at 530 °C for different times are shown in Figure 4.14. It can be found that the first three endothermic peaks are not obvious after 1 h of solution treatment at 530 °C, which manifests the potential of this solution temperature to dissolve the Al_2Cu, Al_2CuMg, and Al_7Cu4Ni phases. However, based on the previous microstructure observations, 5 h of solution treatment at 530 °C is recommended for the AA2618 alloy to make these phases fully dissolved into the Al matrix. The $Al_7Cu_2(Fe,Ni)$ and Al_9FeNi phases were not significantly affected even after extending the solution treatment holding time up to 12 h.

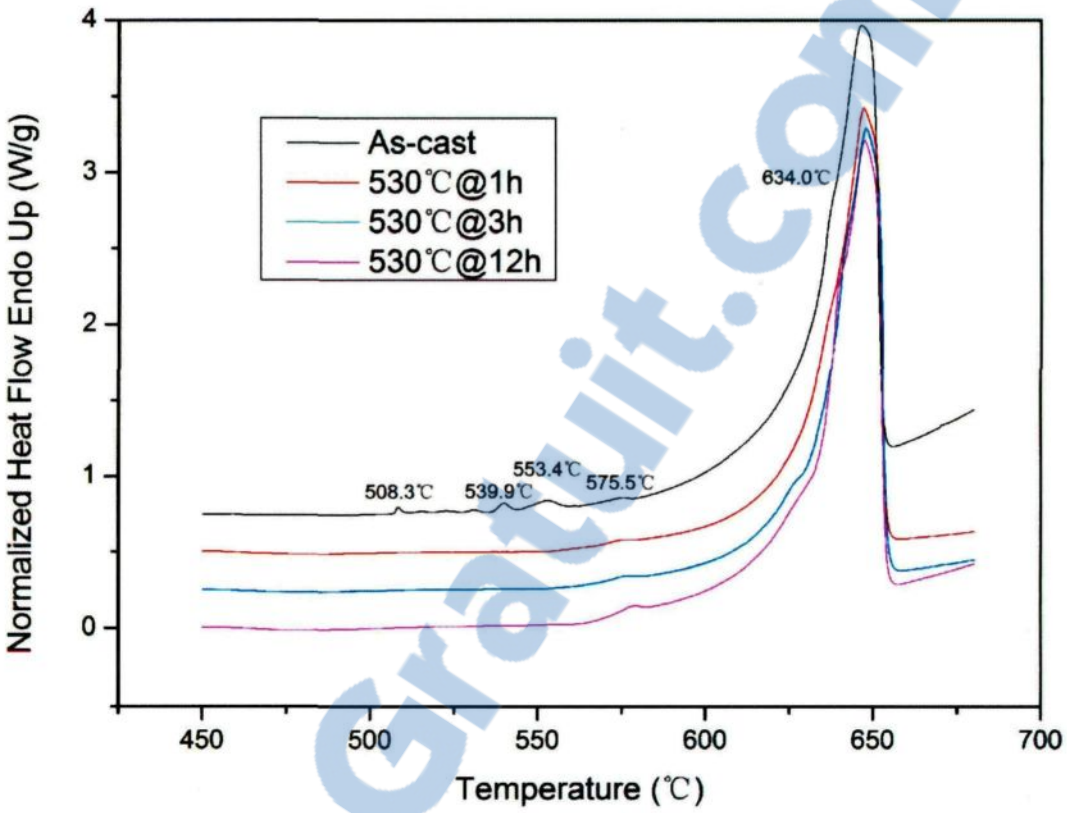

Figure 4.14 DSC heating curves of AA2618 samples solutionized at 530 °C for different times.

4.2.3 Mechanical Properties

This section will discuss the effects of solution treatment and quenching rate on the mechanical properties of the AA2618 alloy. It is important to mention here that, after solution treatment and subsequent quenching, all the mechanical test samples were aged at 200 °C for 20 h.

Figure 4.15 shows the effect of solution temperature on the hardness values of the AA2618 alloy under water quenching and air cooling conditions. The alloy samples were solution treated for 5 h at 480, 505, 530, and 545 °C. As can be seen, the hardness attains the peak value at the solution temperature of 530 °C, where the degree of supersaturation of the solid solution with the strengthening Mg and Cu elements reaches to the maximum, because of the complete dissolution of Al_2Cu, Al_2CuMg, and Al_7Cu_4Ni phases. Due to the insufficient dissolution of strengthening elements, samples treated at solution temperatures of 480 and 505 °C yield relatively lower hardness values. When the solution temperature reaches 545 °C, a minor decrease in the hardness can be observed, which is ascribed to the overheating caused during the solution treatment.

The maximum hardness values for the surface and center water-quenched samples are 95.8 and 94.4 HRF respectively, while those for the air-cooled samples are 88.3 and 86.8 HRF respectively. The lower hardness values in center samples were due to the low content of strengthening elements caused by macrosegregation during the casting process. The air cooled samples exhibit far lower hardness values than those of the water-quenched samples, which confirms that the quenching rate has a significant impact on the age-hardening effect. At higher quenching rates, the atoms of the strengthening elements can be preserved in the solid solution with a higher degree, which would form

finer and more dispersive precipitates during the following aging process, thereby resulting in better mechanical properties.

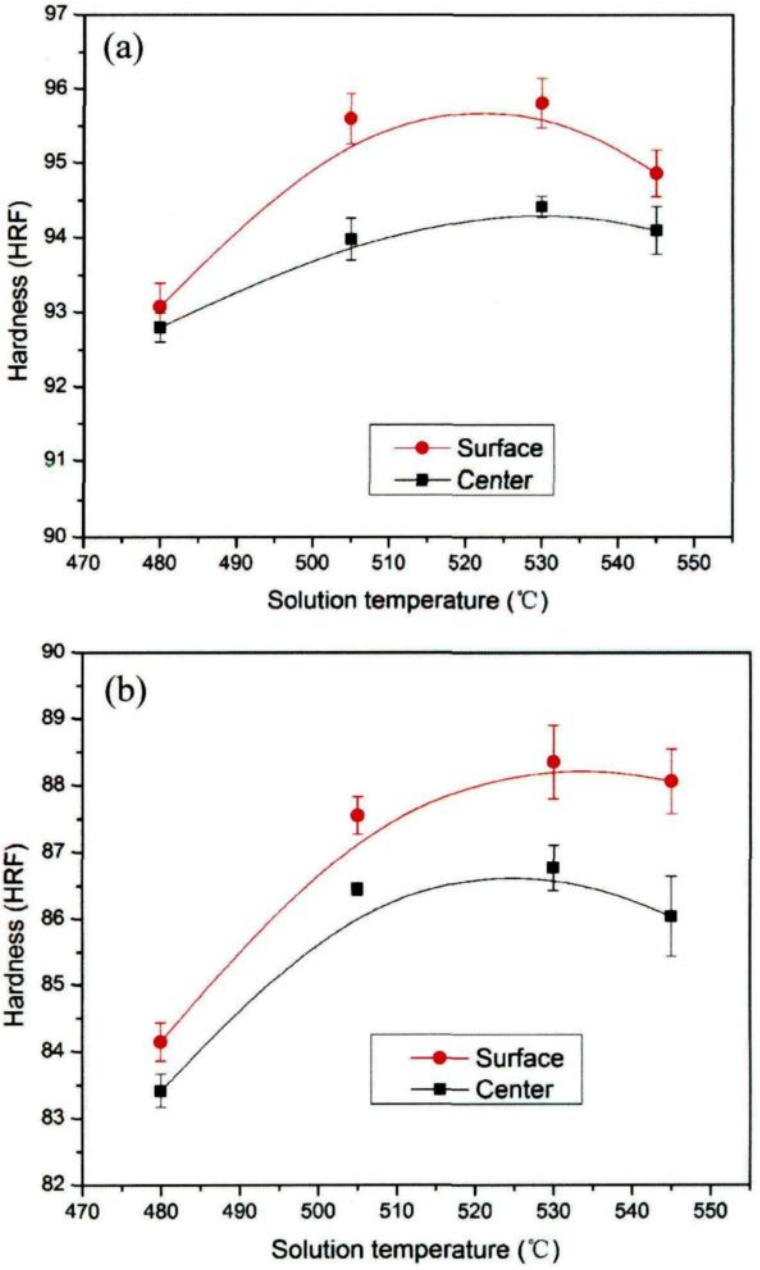

Figure 4.15 Hardness vs. solution temperature curves of AA2618 alloy solution treated for 5 h: (a) water quenched samples; (b) air cooled samples.

Figure 4.16 shows the hardness curves of surface and center AA2618 alloy samples solution treated at 530 °C for different times under water quenching condition. The hardness increases with the solution time up to 5 h, and then slightly decreases with extending the solution time up to 12 h. Solution treatment at 530 °C for 1 or 3 h is not long enough to dissolve all the strengthening elements completely into the solid solution, which results in insufficient precipitate strengthening effect and lower hardness values after aging treatment.

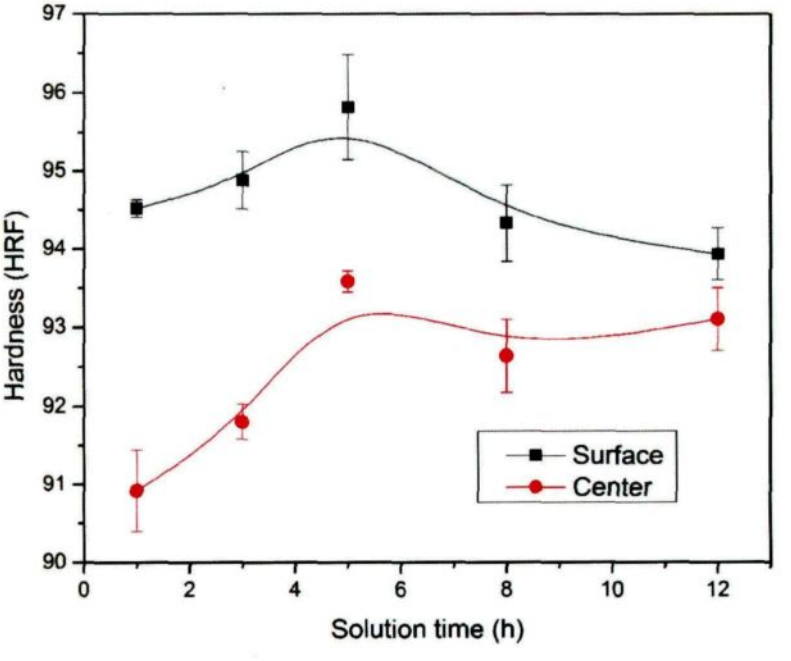

Figure 4.16 Hardness vs. solution time curves of the AA2618 alloy solutionized at 530 °C.

Figure 4.17 demonstrates the tensile properties of the AA2618 alloy for different solution treatment and quenching conditions. It is obvious that both the ultimate and yield strengths are improved greatly after heat treatments attaining approximately twice those in as-cast condition. Increasing the solution temperature from 480 °C to 530 °C increased the YS, UTS and %El by 4.85%, 9.65%, and 13.16%, respectively. Increasing the solution temperature further to 545 °C did not bring about much improvement in the YS and UTS and decreased the %El by 4.05%. This observation can be explained in the light of the harmful overheating caused by this high solution temperature.

With regard to the effect of the quenching rate, it is evident that the yield and tensile strengths of the air cooled sample (258.70 MPa and 329.46 MPa, respectively) are significantly lower than those of the water quenched sample (304.60 MPa and 358.74 MPa, respectively) for the same solution treatment condition, 530 °C for 5 h. However, the air cooling could achieve better elongation rate (17.37%) compared to the water quenching (16.43%).

When the soaking time increased from 5 h to 12 h at 530 °C, both the yield and tensile strengths were not considerably affected, while the elongation rate increased slightly from 16.43% to 17.43%, respectively. Based on the microstructure observations

and the results of the mechanical properties, the solution treatment carried out at 530 °C for 5 h can be deemed as an optimum solution treatment for the non-deformed AA2618 alloy.

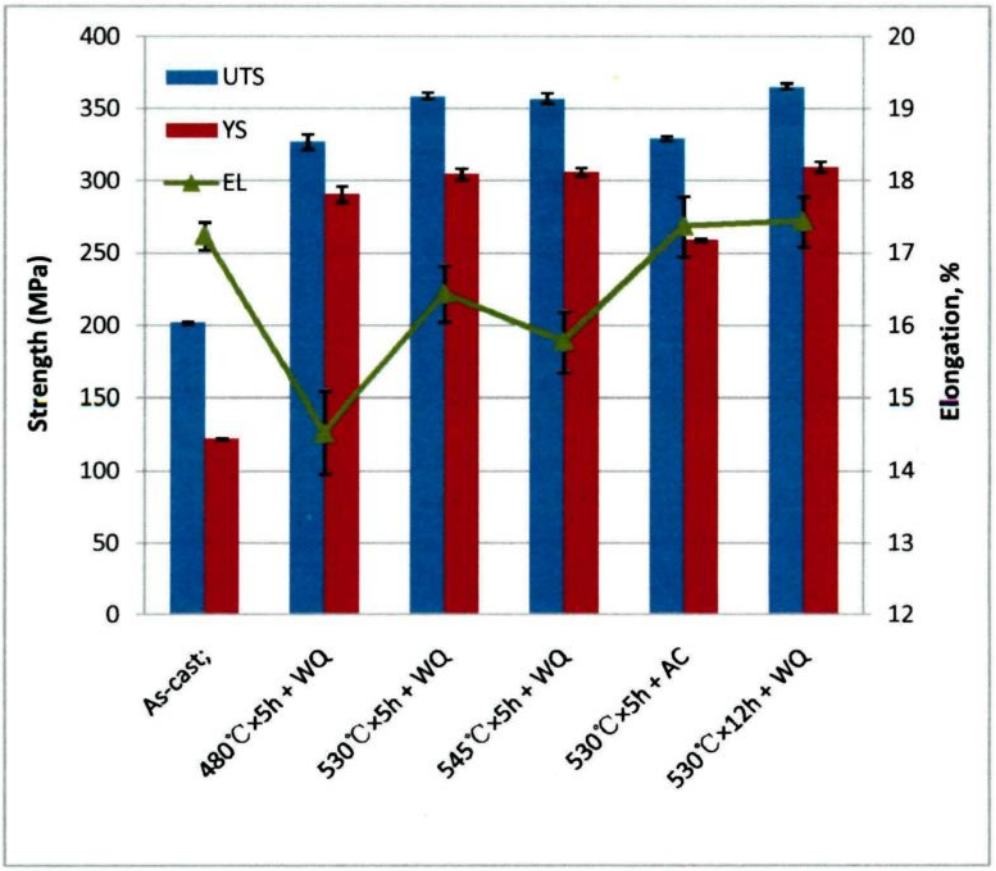

Figure 4.17 Mechanical properties of AA2618 alloy solution treated and quenched under different conditions (WQ: water quenching; AC: air cooling).

4.3 Quench Sensitivity of the AA2618 Alloy

Figure 4.18 shows the cooling curves of the Jominy end quenched cylindrical bar, in

which the distances corresponding to the thermocouples' positions, namely A to G, were measured from the quench end of the test bar. According to the DSC curve shown in Figure 4.26, the quench sensitive temperature range of the AA2618 alloy, within which *S* phase would precipitate rapidly, is between 350 °C and 230 °C. Therefore, the average cooling rates during the temperature interval from 350 °C to 230 °C were calculated for the specified thermocouples positions and the corresponding hardness values were measured in order to determine the effect of cooling rate on the hardness of the AA2618 alloy.

Table 4.2 lists the average cooling rates as computed from the curves shown in Figure 4.18. It is evident from Figure 4.19 that the cooling rate decreases rapidly from 63.49 to 1.29 °C/s with increasing the distance from the quench end. The hardness also exhibits the same declining tendency as the cooling rate, which implies that the hardness of the AA2618 alloy is closely related to the cooling rate. However, the declining level of the hardness value is not so significant, from 102.25 to 99.85 HRF. Therefore, it can be concluded that the hardness of AA2618 alloy has a declining tendency with the decreasing quenching rate, while the declining level is not so significant within the quenching rate range in the present study.

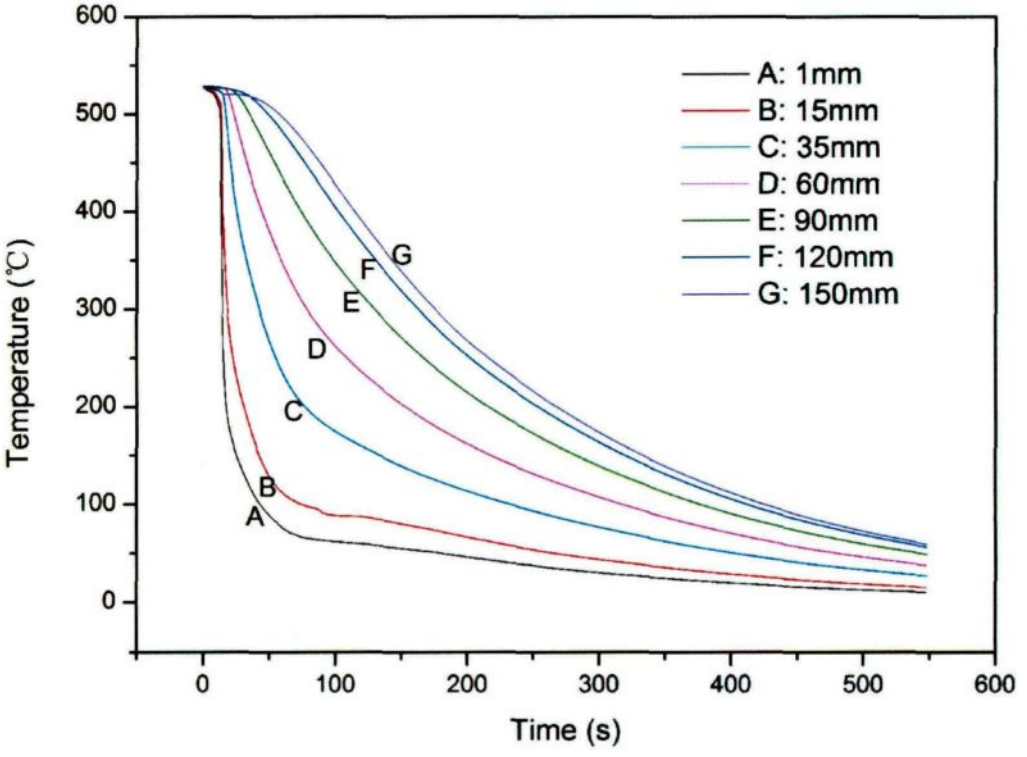

Figure 4.18 Cooling curves of the Jominy end quenched cylindrical bar (A to G refer to the thermocouples' positions).

Table 4.2 Average cooling rates computed from the curves shown in Figure 4.18 in the temperature range between 350 °C and 230 °C.

Identification	A	B	C	D	E	F	G
Distance (mm)	1	15	35	60	90	120	150
Average cooling rate (°C/s)	63.49	13.11	4.10	1.83	1.40	1.32	1.29

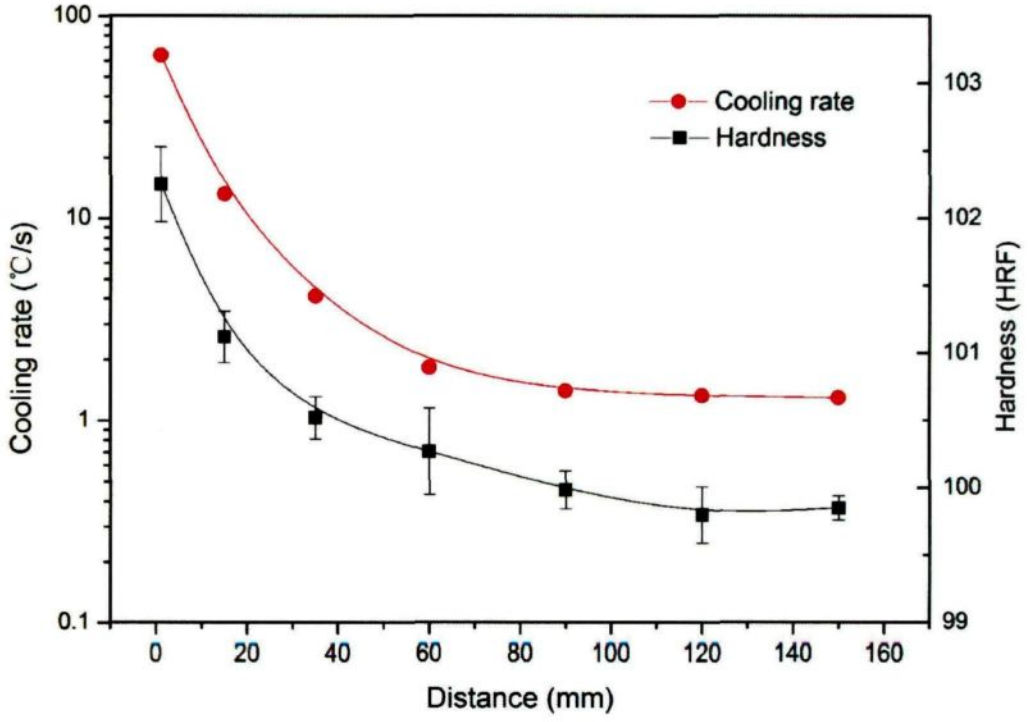

Figure 4.19 The average cooling rate in the temperature interval from 350 °C to 230 °C, and the variation of hardness as a function of the distance to the quench end.

4.4 Effects of aging treatments

4.4.1 Mechanical Properties

Figure 4.20 (a) shows the variation in the hardness values of surface samples of the AA2618 alloy as a function of aging temperature and time. It can be observed that the maximum alloy hardness of 100.0 HRF was obtained after 36 h of aging at 175 °C. At this temperature, the alloy could also display hardness values quite close to this peak

hardness, after aging for 48 h. Increasing the aging temperature to 195 °C shortened the time to reach the peak hardness to 10 h. However, the peak hardness value was decreased (97.4 HRF) when compared to aging condition at 175 °C. It is interesting to note, for both aging conditions at 175 and 195 °C, that the hardness of the AA2618 alloy tend to decrease very slowly after reaching peak hardness contrary to the Al-Cu binary alloys, as shown in Figure 2.9. This observation indicates that AA2618 alloy is not very susceptible to overaging, which may be due to the low coarsening tendency of its main strengthening phase, *S*-Al_2CuMg [54, 55]. Aging at 215 °C further shortened the time to peak hardness to 1 h. This aging condition achieved a peak hardness value (96.8 HRF) slightly lower than that obtained by aging at 195 °C. Prolonged aging at 215 °C beyond 4 h seems to lead to a rapid decline in the hardness as compared to aging conditions at 175 and 195 °C. As shown in Figure 4.20 (b), the hardness values of the center samples are lower than that of surface samples, while they both exhibit the same aging tendency. The peak hardness values of the center samples aged at 175, 195 and 215 °C are 97.5, 95.5 and 94.8 HRF, respectively.

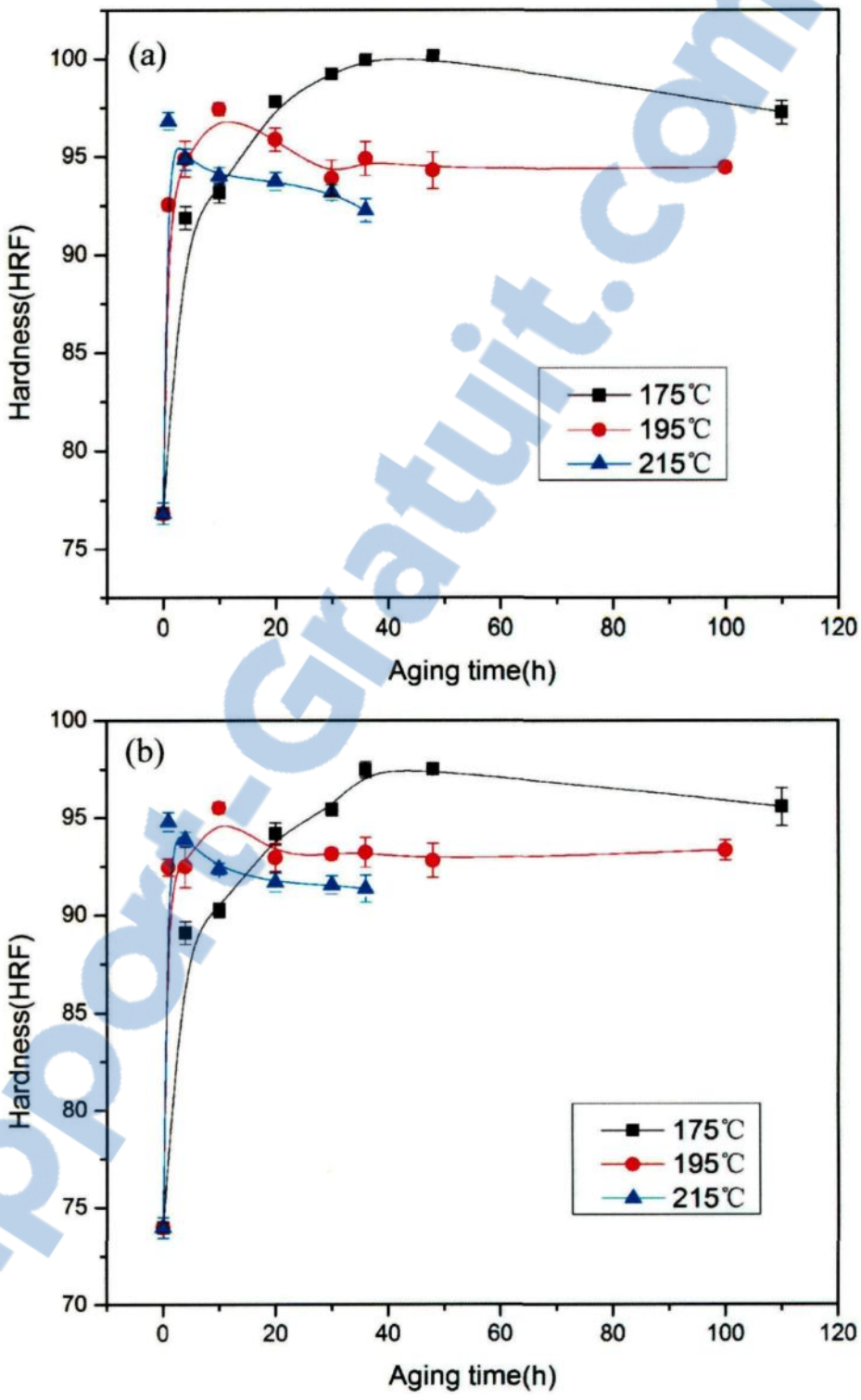

Figure 4.20 Hardness vs. aging time curves of AA2618 alloy aged at 175, 195 and 215 °C: (a) surface samples and (b) center samples.

The tendency of the AA2618 alloy to the natural aging was also investigated by aging alloy samples at room temperature for aging times ranging from 10 h to 5 weeks. The corresponding hardness-aging time curves are illustrated in Figure 4.21, revealing that the AA2618 alloy has a high proneness to the natural aging. As can be observed, the hardness of surface samples increases rapidly from 76.8 to 90.3 HRF during the first 24 h, and then continues to increase gradually, reaching 94.5 HRF after 3 weeks. Prolonged natural aging beyond 3 weeks did not cause any significant change in the hardness values and an almost constant hardness plateau was obtained. It is important to note that the peak hardness value obtained by the natural aging is comparable to the peak hardness values achieved after artificial aging at 195 and 215 °C. The hardness values of the surface samples are also slightly higher than that of the center samples, as previously observed in the artificial aging conditions.

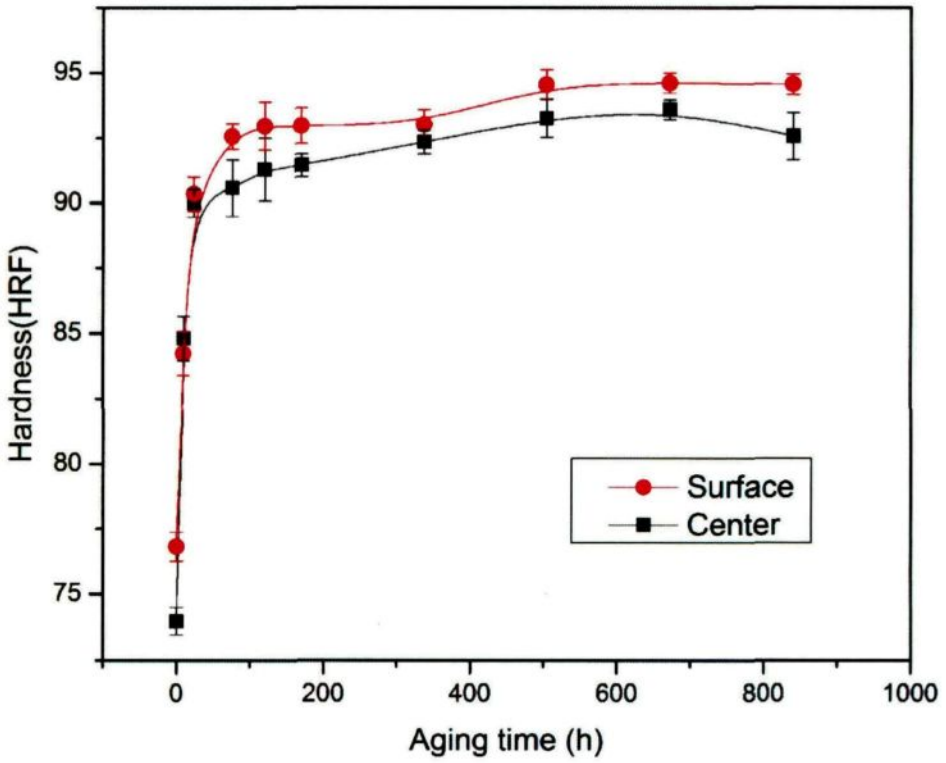

Figure 4.21 Hardness vs. aging time curves of the natural aged AA2618 alloy.

Figure 4.22 displays the tensile properties of the AA2618 alloy for different aging conditions. The variation tendencies of the ultimate and yield strengths are in line with those of the hardness values. The elongation exhibits exactly the reverse tendency to those of the strengths. The maximum YS and UTS values of 395.8 and 422.8 MPa, respectively, were obtained after aging at 175 °C for 36 h. The lowest elongation value of 10.3% is corresponding to the two peak aging conditions at 215 and 195 °C, respectively. It is interesting to note that, the aging treatments applied to the AA2618 alloy could

produce a wide range of satisfactory combinations of strength and ductility, which may fulfill the specifications of the molding plates.

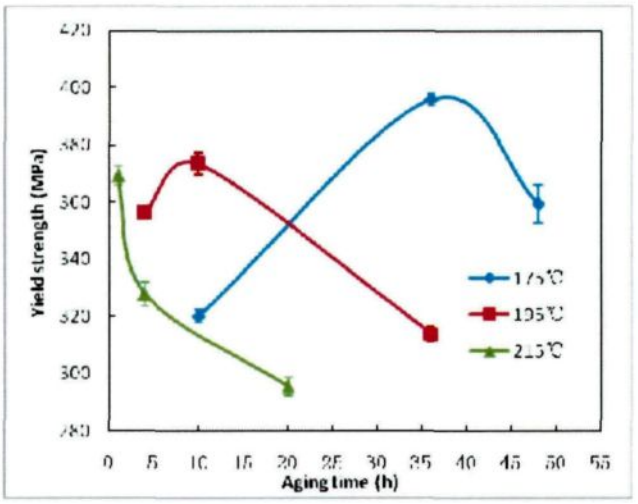

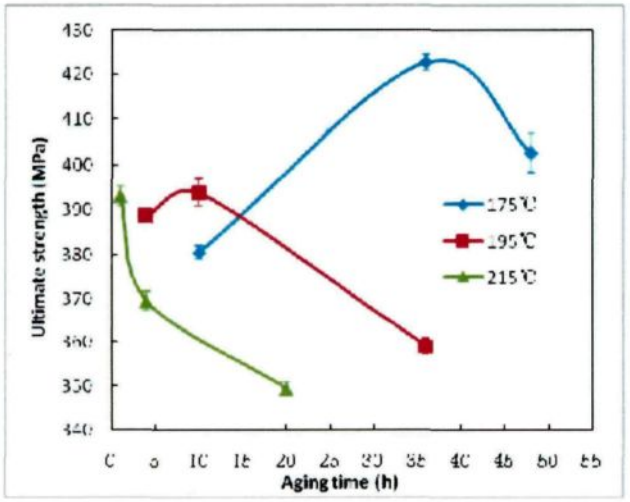

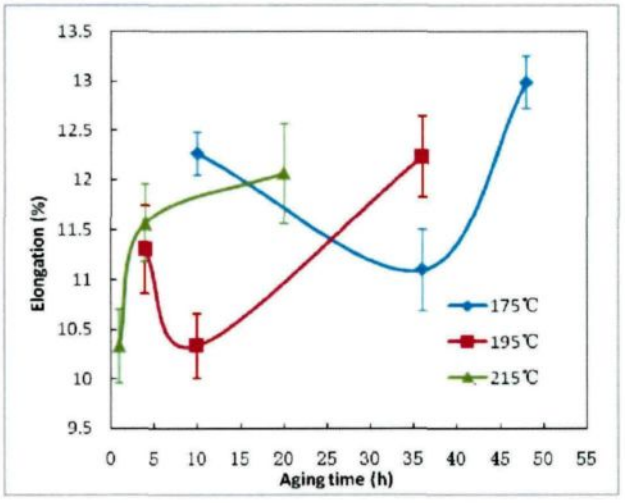

Figure 4.22 Tensile properties of AA2618 alloy under different aging conditions.

4.4.2 Electrical Conductivity

Figure 4.23 shows the variation in the electrical conductivity of the AA2618 alloy as a function of aging time at different isothermal holding temperatures. The value of electrical conductivity of the surface and center samples, in the as-quenched condition, was found to be 35.72 and 36.1 %IACS, respectively. It is obvious that, except an initial decrease caused at 175 °C, the electrical conductivity increases with increasing aging temperature and extending aging time. The increasing rate of the conductivity depends on both the aging temperature and aging time, so that it decreases with decreasing aging temperature and increasing aging time. The slopes of the electrical conductivity curves begin to decrease after aging for 1 h at 215 °C and 10 h at 195 °C, which corresponds to the response of the hardness to the aging time. During the overaging stage, the electrical conductivity increases very slowly, which indicates that the supersaturation degree of the solid solution has been reduced greatly by the aging treatment.

Contrary to the artificial aging, the electrical conductivity of the AA2618 alloy declines with increasing the natural aging time, as shown in Figure 4.24. The conductivity decreases abruptly at the beginning of the natural aging and then becomes extremely sluggish to change with the aging time, displaying an almost constant value of

33.33 and 33.61 %IACS for surface and center samples, respectively.

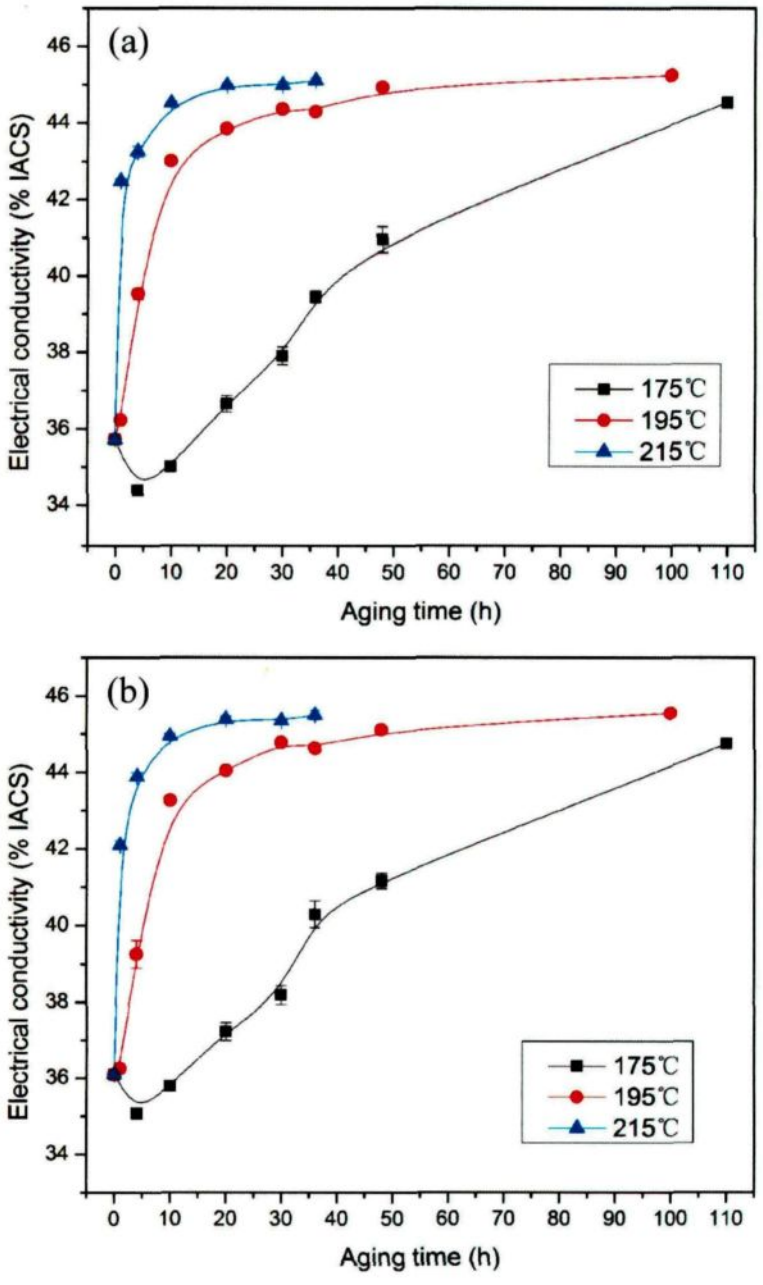

Figure 4.23 Electrical conductivity vs. aging time curves of the AA2618 alloy samples aged at 175 °C, 195 °C and 215 °C: (a) surface samples, and (b) center samples.

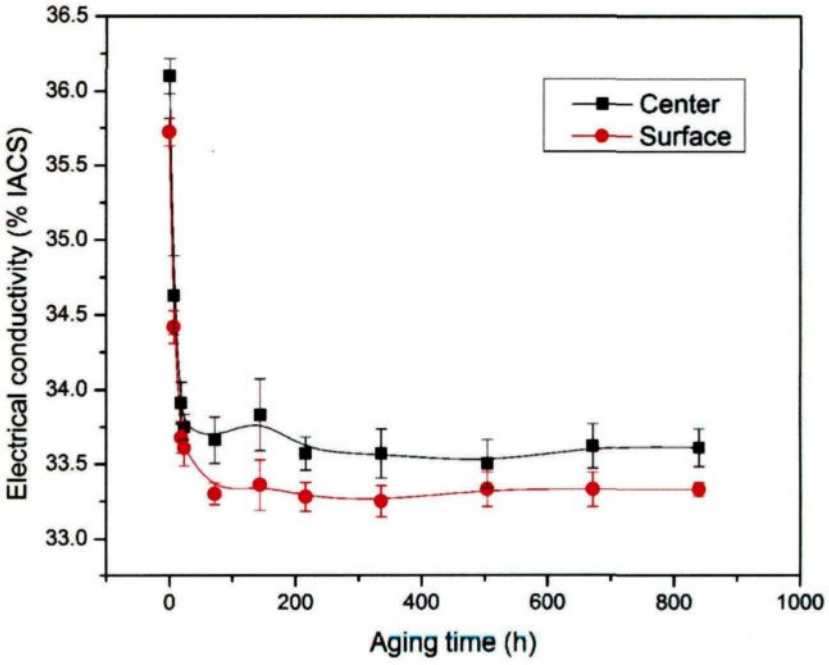

Figure 4.24 Electrical conductivity vs. aging time curves of the as-quenched AA2618 alloy aged at room temperature.

The decrease in the electrical conductivity of the AA2618 alloy, during the first few hours of the artificial aging at 175 °C and after the natural aging, is possibly due to the formation of GPB zones [47]. The effective scattering of electrons by the evenly dispersed GPB zones leads to increase in the electrical resistance, that is, decrease in the electrical conductivity. On the other hand, the formation of GPB zones clusters Cu and Mg atoms, as well as the quenched-in vacancies, thereby purifying the aluminum matrix from potential scatterers of electrons, namely, increasing the electrical conductivity.

However, the purification achieved by the formation of zones is not sufficient to compensate for the opposite effect, namely the effective scattering of electrons by the GPB zones, which in turn results in the reduction observed in the electrical conductivity.

At higher artificial aging temperatures, the GPB zones formed rapidly and cannot persist since the solvus line for the existence of these zones is approached. Consequently, they dissolve back into the matrix by the diffusion process or become nuclei for the formation of strengthening S phase precipitates. As the aging temperature increases, the increasing rate of both electrical conductivity and hardness increases in accordance with the rate of the formation of S phase precipitates. The initial decrease caused in the electrical conductivity at 175 °C was not observed at 195 °C and 215 °C, as shown in Figure 4.23 because the GPB zones formed and then dissolved rapidly at such elevated temperatures. The increase in the electrical conductivity during the artificial aging can be explained in terms of the purification of the aluminum matrix. The solute atoms of Cu and Mg, which act as scatterers of electrons, precipitate out of the aluminum matrix forming S phase. In contrast with GPB zones, the relatively large S phase precipitates scatter electrons to a lesser degree. They increase in size as aging temperature or aging time increase, thus minimizing their scattering effect. The conductivity at 195 °C and 215 °C levels off at a value of 45 % IACS as a result of maximum purification of Cu and

Mg atoms.

The hardness versus electrical conductivity curve, which exhibit a C-shape, is shown in Figure 4.25. For the natural aging and over aging conditions, the hardness varies inversely with the electrical conductivity. For the under and peak aging conditions, the hardness increases proportionally with the electrical conductivity.

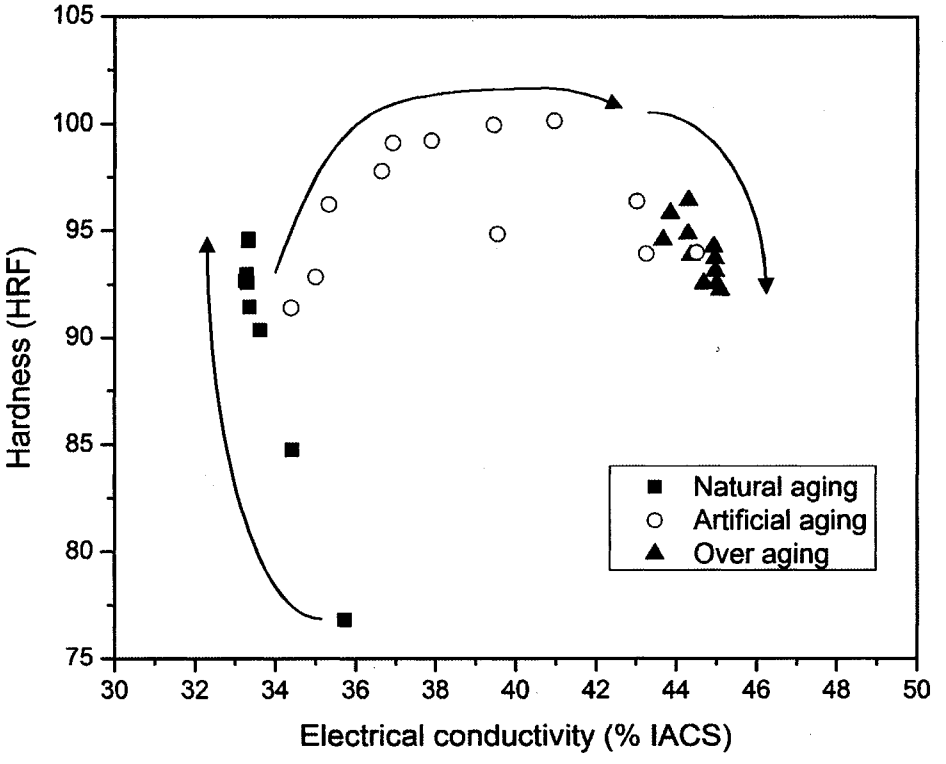

Figure 4.25 Hardness versus electrical conductivity profile of the AA2618 alloy for different aging conditions.

4.4.3 DSC Analysis

Figure 4.26 to Figure 4.29 show the DSC curves of the AA2618 alloy in as-quenched and different artificial aging conditions. Three main peaks may be identified in these thermograms [33, 38]: an endothermic peak, A, between 180 and 240 °C, attributed to the dissolution of GPB zone; an exothermic peak, B, between about 240 and 320 °C, representing the formation of *S* phase precipitates and a broad endothermic peak, C, between 340 and 480 °C, corresponding to the progressive dissolution of the *S* precipitates [36].

The DSC curves reveal that both the dissolution peak of GPB zones and the formation peak of S phase decrease with extending aging time (Figure 4.26 and Figure 4.27) and increasing aging temperature (Figure 4.29). This means that the samples aged for longer times or at higher aging temperatures contained less GPB zones and more S phase precipitates, that is, more GPB zones were transformed to the main strengthening contributor S phase [33].

For aging at 175 °C, the heat flow of peaks A and B decrease with increasing aging time from 4 h to 36 h, as shown in Figure 4.26. It is obvious that peak A for the sample aged for 4 h is higher than that for the sample aged for 36 h, which indicates that there are

plenty of GPB zones formed initially after aging for 4 h at 175 °C. These zones contribute to a large extent to the strengthening effect produced by this aging condition. On the other hand, after 36 h of aging, the significant reduction in heat flow of peaks A and B implies that a large amount of GPB zones had already transformed to *S* phase.

It can be observed from Figure 4.27 and Figure 4.28 that, after aging at 195 °C for 10 h and 215 °C for 1 h, the *S* phase formation peak, B, almost disappeared. This observation implies that the age hardening at these two aging conditions is mainly dominated by *S* phase, which forms dense precipitates at the peak hardness stage. Wang *et al.* [33] and Lu *et al.* [16] used the TEM to study the precipitation sequence after artificial aging of Al-Cu-Mg and AA2618 alloys and concluded that besides *S* phase, no significant amounts of other phases or zones were detected at the peak hardness stage.

It can be found that after aging 36 h at 175 °C, which was concluded as the peak aging condition previously, the *S* phase formation peak did not completely disappear as the peak aged conditions at 195 and 215 °C. According to precipitates hardening theory, the hardening effect depends on both the volume fraction and size of the precipitates. So the aging behavior of aluminum alloys is closely related to the precipitating rate and coarsening rate. It can be presumed that, at relatively low temperature 175 °C, the

precipitating rate is lower than the coarsening rate of the precipitates, which leads to the decline of the mechanical properties of the AA2618 alloy sample aged for 48 h.

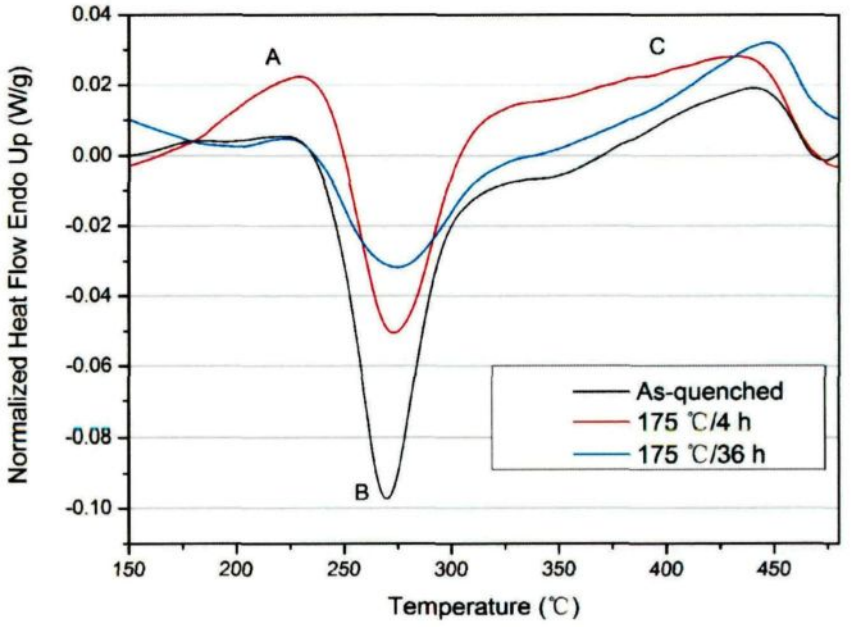

Figure 4.26 DSC curves of the AA2618 alloy in the as-quenched condition and after aging at 175 °C for 4 and 36 h.

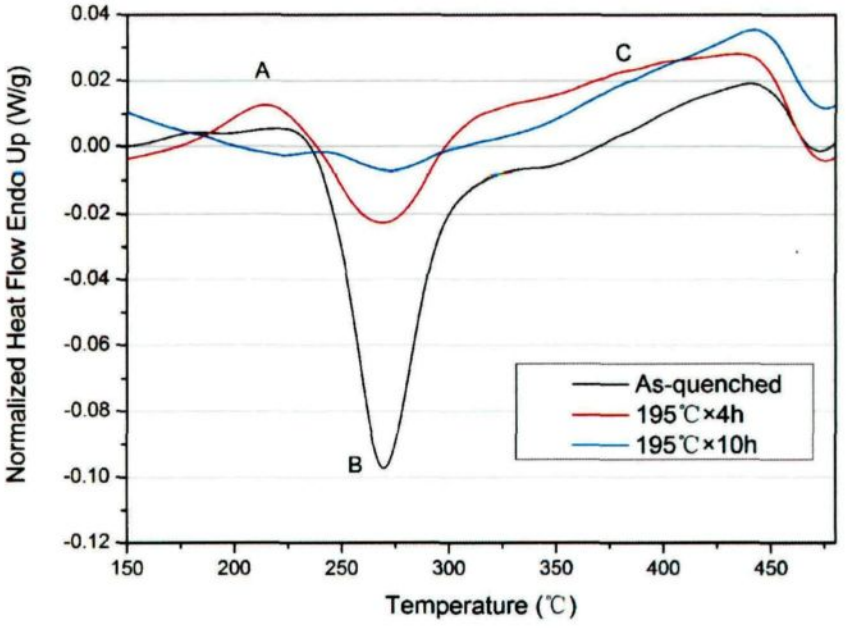

Figure 4.27 DSC curves of the AA2618 alloy in the as-quenched condition and after aging at 195 °C for 4 and 10 h.

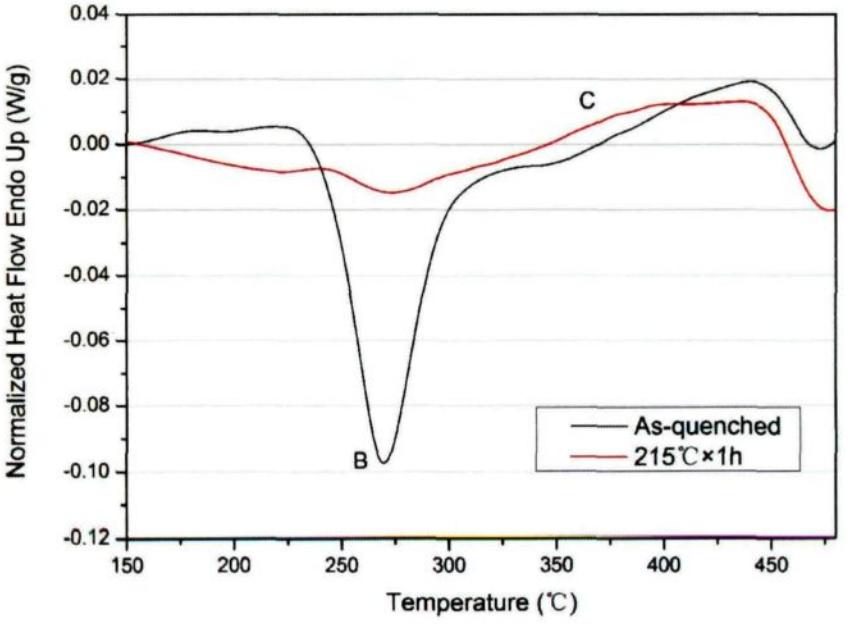

Figure 4.28 DSC curves of the AA2618 alloy in the as-quenched condition and after aging at 215 °C for 1 h.

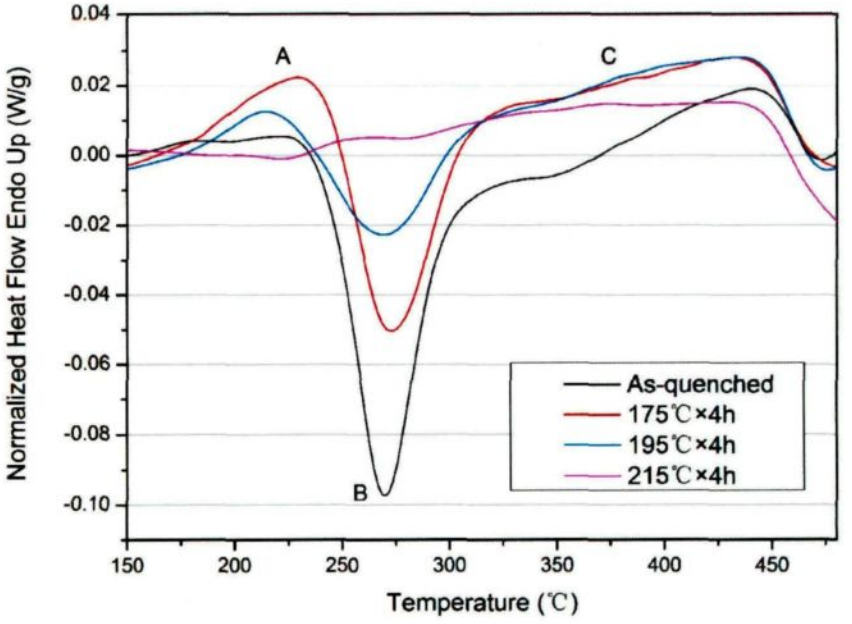

Figure 4.29 DSC curves of the AA2618 alloy in the as-quenched condition and after aging for 4 h at different temperatures.

Figure 4.30 shows the DSC curves of the AA2618 alloy samples aged at room temperature for different times. Besides the three thermal effects mentioned above, another endothermic effect (labeled a) in temperature range from 150 °C to 180 °C can be identified, which may be attributed to the dissolution of co-clusters of Cu and Mg. Due to the extremely slow precipitation speed and the lower temperature during natural aging, the precipitated co-clusters could be retained, while it could hardly be found during artificial aging process. The DSC curves also reveal that the formation peak of *S* phase has only a slight decline after natural aging for up to 5 week, which indicates that there is

rarely *S* phase formed during the natural aging process. It can be suggested that the natural aging hardening is dominated by the co-clusters and GPB zones.

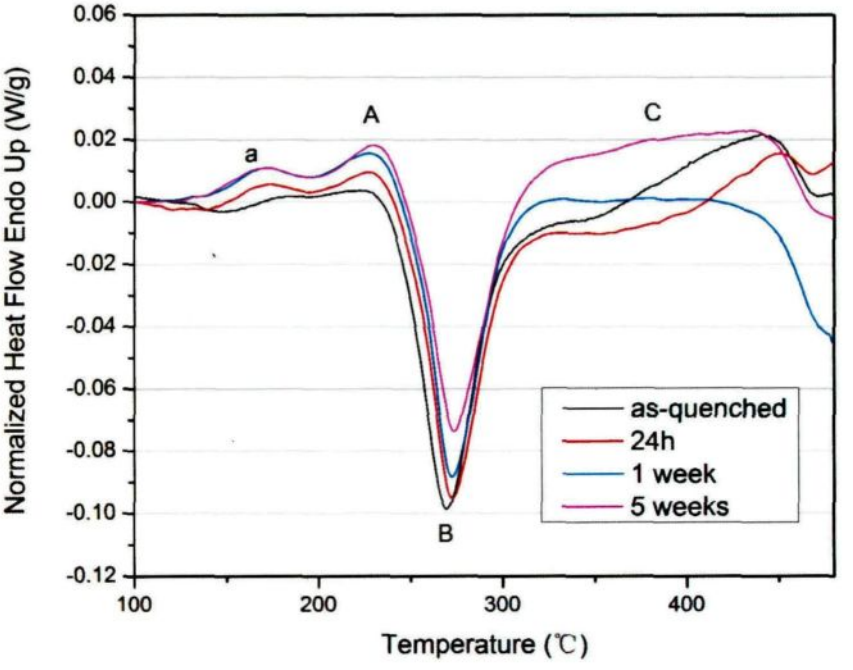

Figure 4.30 DSC curves of the AA2618 alloy in the as-quenched condition and after aging at room temperature for different times.

5 CONCLUSIONS AND RECOMMENDATIONS

5.1 Conclusions

An investigation was carried out on the effects of the heat treatment on the microstructure and mechanical properties of the AA2618 DC cast alloy proposed for the manufacturing of precision molding plates. Based on the results obtained, the following conclusions can be drawn:

(1) The microstructure of the as-cast AA2618 alloy is composed of Al_2Cu, Al_2CuMg, Al_7Cu_4Ni, $Al_7Cu_2(Fe,Ni)$, and Al_9FeNi intermetallic phases, distributed at α-Al dendrite boundaries.

(2) The solution treatment carried out at 530 °C for 5 h was found to be the optimum solution treatment, by which the Al_2CuMg, Al_2Cu and Al_7Cu_4Ni phases could be dissolved completely into the solid solution, whereas the $Al_7Cu_2(Fe,Ni)$ and Al_9FeNi phases were only subjected to fragmentation and spheroidization.

(3) The effect of solution soaking time on the microstructure and mechanical properties of the AA2618 alloy is not as significant as that of the solution temperature.

(4) AA2618 alloy is a quench sensitive aluminum alloy. With the same solution and aging conditions, the air-cooled samples yields lower hardness and strength values than water-quenched samples. The Jominy end quench test results demonstrated that the hardness value of the AA2618 alloy declines with decreasing cooling rate.

(5) The peak-aged conditions of the AA2618 alloy were attained after aging for 36 h at 175 °C, 10 h at 195 °C and 1 h at 215 °C with surface hardness values of 100.0, 97.4 and 96.8 HRF, and center hardness values of 97.5, 95.5 and 94.8 HRF, respectively.

(6) The aging treatments applied to the AA2618 alloy result in different combinations of strength and ductility, which may satisfactorily fulfill the specifications of the large mold manufacturers.

(7) AA2618 alloy was found to be prone to the natural aging, displaying hardness

values comparable to those obtained by the artificial aging at 195 and 215 °C.

(8) DSC analysis suggested that the main strengthening phase of the AA2618 alloy, under artificial aging, is *S*-Al_2CuMg phase, whereas the strengthening effect caused by the natural aging is probably attributed to the formation of Cu-Mg co-clusters and/or GPB zones.

(9) The electrical conductivity of the AA2618 alloy decreased during the first 4 hours of aging at 175 °C and during the whole natural aging process, due to the formation of GPB zones and increased over other artificial aging periods, due to the purification of the aluminum matrix.

5.2 Recommendations for the future works

(1) Quench sensitivity test at much lower cooling rates can be further studied to reveal the relationship between mechanical properties of the AA2618 alloy and lower quenching rates.

(2) Presently, the internal residual stress of AA2618 alloy induced after solution treatment and quenching is still a problem affecting the dimensional stability of the final cast plates. This problem is very essential to the practical production

and needs more investigation work to be done. The effects of heat treatment procedures (solution treatment, quenching, and aging) on the residual stress developed in the AA2618 cast plates may therefore be recommended to study by implementing such residual stress measurement techniques as ultrasonic, X-ray diffraction, crack compliance, and hole drilling methods.

REFERENCES

1. I. J. Polmear, *Light alloys : metallurgy of the light metals.* (J. Wiley & Sons, New York, 1995).

2. American Society for Metals, *ASM handbook. Volume 2, Properties and selection: nonferrous alloys and special-purpose materials.* (ASM International, Materials Park, OH, 1990).

3. I. Özbek, A study on the re-solution heat treatment of AA 2618 aluminum alloy. *Materials Characterization* **58**, 312 (2007).

4. American Society for Metals, *ASM handbook. Volume 2, Properties and selection : nonferrous alloys and special-purpose materials.* (American Society for Metals, Metals Park, Ohio, 1979).

5. J. G. Kaufman, *Properties of aluminum alloys: tensile, creep, and fatigue data at high and low temperatures.* (ASM International ; Aluminum Association, Materials Park, Ohio; Washington, D.C., 1999).

6. J. E. Hatch, Aluminum Association, American Society for Metals, *Aluminum : properties and physical metallurgy.* (American Society for Metals, Metals Park, Ohio, 1984).

7. R. A. Higgins, *Engineering metallurgy part I : Applied physical metallurgy.* (R.E. Krieger Pub. Co., Malabar, Fla., 1983).

8. E. C. Rollason, in *Metallurgy for engineers.* (Edward Arnold, London, 1973), pp. 277-279.

9. R. N. Wilson, P. J. E. Forsyth, Effects of Additions of 1% Iron and 1%

Nickel on Age-hardening of an Aluminum-2.5%Copper-1.2%Magnesium Alloy. *Journal of the institute of metals* **94**, 8 (1966).

10. R. P. Underhill, P. S. Grant, B. Cantor, MICROSTRUCTURE OF SPRAY-FORMED AL ALLOY-2618. *Materials & Design* **14**, 45 (Feb, 1993).

11. W. Feng, X. Baiqing, Z. Yongan, L. Zhihui, L. Peiyue, Microstructural characterization of an Al-Cu-Mg alloy containing Fe and Ni. *Journal of Alloys and Compounds* **487**, 445 (2009).

12. G. Wang, B. Xiong, Y. Zhang, Z. Li, P. Li, Microstructural characterization of as-cast and homogenized 2D70 aluminum alloy. *International Journal of Minerals, Metallurgy and Materials* **16**, 427 (2009).

13. I. N. A. Oguocha, S. Yannacopoulos, Y. Jin, The structure of AlxFeNi phase in Al-Cu-Mg-Fe-Ni alloy (AA2618). *Journal of Materials Science* **31**, 5615 (1996).

14. S. C. Bergsma, X. Li, M. E. Kassner, Effects of thermal processing and copper additions on the mechanical properties of aluminum alloy ingot AA 2618. *J. Mater. Eng. Perform.* **5**, 100 (Feb, 1996).

15. R. N. Wilson, D. M. Moore, P. J. E. Forsyth, EFFECTS OF 3.25 PERCENT SILICON ON PRECIPITATION PROCESSES IN AN ALUMINIUM-2.5 PERCENT COPPER-1.2 PERCENT MAGNESIUM ALLOY. *Journal of the institute of metals* **95**, 177 (1967).

16. H. Lu, P. Kadolkar, K. Nakazawa, T. Ando, C. A. Blue, Precipitation behavior of AA2618. *Metall. Mater. Trans. A-Phys. Metall. Mater. Sci.* **38A**, 2379 (Oct, 2007).

17. J. H. Wang, D. Q. Yi, B. Wang, Microstructure and properties of 2618-Ti heat resistant aluminum alloy. *Trans. Nonferrous Met. Soc. China* **13**, 590 (Jun, 2003).

18. K. Yu, W. Li, S. Li, J. Zhao, Mechanical properties and microstructure of aluminum alloy 2618 with Al3(Sc, Zr) phases. *Materials Science and Engineering*

A **368**, 88 (2004).

19. K. R. Van Horn, *Aluminum. vol.1, properties, physical metallurgy and phase diagrams.* (American Society for Metals, Metals Park (Ohio), 1967).

20. X. Y. Liu *et al.*, Effects of solution treatment on the microstructure and mechanical properties of Al-Cu-Mg-Ag alloy. *Materials & Design* **31**, 4392 (2010).

21. W. A. Anderson, in *Precipitation from Solid Solution,* A. S. f. Metals, Ed. (1959), pp. 150-207.

22. M. Tiryakioğlu, R. T. Shuey, Quench sensitivity of 2219-T87 aluminum alloy plate. *Materials Science and Engineering: A* **527**, 5033 (2010).

23. I. N. A. Oguocha, M. Radjabi, S. Yannacopoulos, The effect of cooling rate on the quench sensitivity of 2618 Al/Al2O3 MMC. *Journal of Materials Science* **35**, 5629 (2000).

24. J. W. Newkirk, D. S. MacKenzie, The Jominy end quench for light-weight alloy development. *J. Mater. Eng. Perform.* **9**, 408 (Aug, 2000).

25. J. L. Cavazos, R. Colás, Quench sensitivity of a heat treatable aluminum alloy. *Materials Science and Engineering: A* **363**, 171 (2003).

26. C. Oksuz, O. Sen, R. Bozdogan, M. Cigdem, Quench Sensitivity of Medium and High Strength Aluminium Alloys. *Mater. Test.-Mater. Compon. Techn. Appl.* **52**, 367 (2010).

27. W. E. Jominy, A. L. Boegehold, *ASM Trans.* **27**, (1939).

28. B. M. Loring, W. H. Baer, G. M. Carlton, THE USE OF THE JOMINY TEST IN STUDYING COMMERCIAL AGE-HARDENING ALUMINUM ALLOYS. *Transactions of the American Institute of Mining and Metallurgical Engineers* **175**, 401 (1948).

29. H. K. Hardy, THE AGEING CHARACTERISTICS OF BINARY ALUMINIUM-COPPER ALLOYS. *Journal of the institute of metals* **79**, 321 (1951).

30. Y. A. Bagaryatsky, Structural changes on aging Al-Cu-Mg alloys. *Dokl. Akad. Nauk SSSR* **87**, 397 (1952).

31. J. M. Silcock, THE STRUCTURAL AGEING CHARACTERISTICS OF AL-CU-MG ALLOYS WITH COPPER-MAGNESIUM WEIGHT RATIOS OF 7-1 AND 2.2-1. *Journal of the institute of metals* **89**, 203 (1961).

32. H. Perlitz, A. Westgren, The crystal structure of Al_2CuMg. *Ark. Kemi, Mineral. Geol.* **16 B**, 1 (1943).

33. S. C. Wang, M. J. Starink, N. Gao, Precipitation hardening in Al-Cu-Mg alloys revisited. *Scr. Mater.* **54**, 287 (Jan, 2006).

34. S. C. Wang, M. J. Starink, Two types of S phase precipitates in Al-Cu-Mg alloys. *Acta Mater.* **55**, 933 (Feb, 2007).

35. S. P. Ringer, K. Hono, T. Sakurai, I. J. Polmear, Cluster hardening in an aged Al-Cu-Mg alloy. *Scr. Mater.* **36**, 517 (1997).

36. M. J. Starink, N. Gao, J. L. Yan, The origins of room temperature hardening of Al-Cu-Mg alloys. *Materials Science and Engineering a-Structural Materials Properties Microstructure and Processing* **387**, 222 (Dec, 2004).

37. S. P. Ringer, S. K. Caraher, I. J. Polmear, Response to comments on cluster hardening in an aged Al-Cu-Mg alloy. *Scr. Mater.* **39**, 1559 (1998).

38. N. Gao, L. Davin, S. Wang, A. Cerezo, M. J. Starink, in *Aluminum Alloys 2002: Their Physical and Mechanical Properties Pts 1-3,* P. J. Gregson, S. J. Harris, Eds. (Trans Tech Publications Ltd, Zurich-Uetikon, 2002), vol. 396-4, pp. 923-928.

39. B. Klobes, K. Maier, T. E. M. Staab, Natural ageing of Al–Cu–Mg revisited from a local perspective. *Materials Science and Engineering: A* **528**, 3253 (2011).

40. J. Wang, D. Yi, X. Su, F. Yin, Influence of deformation ageing treatment on microstructure and properties of aluminum alloy 2618. *Materials Characterization* **59**, 965 (2008).

41. F. Novy, M. Janecek, R. Kral, Microstructure changes in a 2618 aluminium alloy during ageing and creep. *Journal of Alloys and Compounds* **487**, 146 (2009).

42. P. Villars, A. Prince, H. Okamoto, *Handbook of ternary alloy phase diagrams.* (ASM International, [Materials Park, OH], 1995).

43. D. Turnbull, H. S. Rosenbaum, H. N. Treaftis, KINETICS OF CLUSTERING IN SOME ALUMINUM ALLOYS. *Acta Metallurgica* **8**, 277 (1960).

44. K. M. Entwistle, K. I. Koo, J. H. Fell, EFFECT OF VACANCY/IMPURITY INTERACTION ON RATE OF QUENCH-AGE-HARDENING IN ALUMINIUM-COPPER ALLOYS. *Journal of the institute of metals* **91**, 84 (1962).

45. Y. Gefen, M. Rosen, A. Rosen, AGING PHENOMENA IN DURALUMINUM 2024 STUDIED BY RESISTOMETRY AND HARDNESS. *Materials Science and Engineering* **8**, 181 (1971).

46. P. L. Rossiter, P. Wells, ELECTRICAL RESISTIVITY DURING PRE-PRECIPITATION PROCESSES. *Philosophical Magazine* **24**, 425 (1971).

47. M. Rosen, E. Horowitz, L. Swartzendruber, S. Fick, R. Mehrabian, The aging process in aluminum alloy 2024 studied by means of eddy currents. *Materials Science and Engineering* **53**, 191 (1982).

48. C. H. Gur, I. Yildiz, Utilization of Non-destructive Methods for Determining the Effect of Age-Hardening on Impact Toughness of 2024 Al-Cu-Mg Alloy. *Journal of Nondestructive Evaluation* **27**, 99 (Dec, 2008).

49. C. H. Gur, I. Yildiz, Non-destructive investigation on the effect of precipitation hardening on impact toughness of 7020 Al-Zn-Mg alloy. *Materials Science and Engineering a-Structural Materials Properties Microstructure and Processing* **382**, 395 (Sep, 2004).

50. C. Panseri, T. Federighi, A RESISTOMETRIC STUDY OF PRE-PRECIPITATION IN AL-10-PERCENT ZN. *Acta Metallurgica* **8**, 217 (1960).

51. F. Tariq, N. Naz, R. Baloch, F. Faisal, Characterization of Material Properties of 2xxx Series Al-Alloys by Non Destructive Testing Techniques. *Journal of Nondestructive Evaluation* **31**, 17 (2012).

52. E. W. Lee *et al.*, The effect of thermal exposure on the electrical conductivity and static mechanical behavior of several age hardenable aluminum alloys. *Eng. Fail. Anal.* **14**, 1538 (Dec, 2007).

53. M. A. Salazar-Guapuriche, Y. Y. Zhao, A. Pitman, A. Greene, in *Aluminium Alloys 2006, Pts 1 and 2: Research through Innovation and Technology,* W. J. Poole, M. A. Wells, D. J. Lloyd, Eds. (Trans Tech Publications Ltd, Zurich-Uetikon, 2006), vol. 519-521, pp. 853-858.

54. W. Rainforth, H. Jones, Coarsening of S'-Al2CuMg in Al-Cu-Mg base alloys. *Journal of Materials Science Letters* **16**, 420 (1997).

55. L. M. Rylands, W. M. Rainforth, H. Jones, Coarsening rates of S' precipitates in Al-4.1wt% Cu-1.6wt% Mg alloy during extended treatment at 200 °C. *Philosophical Magazine Letters* **76**, 63 (Aug, 1997).